LOCKHEED MARTIN ENERGY RESEARCH LIBRARIES
3 4456 0515554 1

CENTRAL RESEARCH LIBRARY
DOCUMENT COLLECTION

2

ORNL-4365
UC-4 – Chemistry

CHEMICAL TECHNOLOGY DIVISION

UNIT OPERATIONS SECTION

QUARTERLY PROGRESS REPORT

APRIL – JUNE 1968

OAK RIDGE NATIONAL LABORATORY
CENTRAL RESEARCH LIBRARY
DOCUMENT COLLECTION
LIBRARY LOAN COPY
DO NOT TRANSFER TO ANOTHER PERSON
If you wish someone else to see this document, send in name with document and the library will arrange a loan.
UCN-7969
(3 3-67)

OAK RIDGE NATIONAL LABORATORY
operated by
UNION CARBIDE CORPORATION
for the
U.S. ATOMIC ENERGY COMMISSION

Printed in the United States of America. Available from Clearinghouse for Federal Scientific and Technical Information, National Bureau of Standards, U.S. Department of Commerce, Springfield, Virginia 22151
Price: Printed Copy $3.00; Microfiche $0.65

LEGAL NOTICE

This report was prepared as an account of Government sponsored work. Neither the United States, nor the Commission, nor any person acting on behalf of the Commission:

A. Makes any warranty or representation, expressed or implied, with respect to the accuracy, completeness, or usefulness of the information contained in this report, or that the use of any information, apparatus, method, or process disclosed in this report may not infringe privately owned rights; or

B. Assumes any liabilities with respect to the use of, or for damages resulting from the use of any information, apparatus, method, or process disclosed in this report.

As used in the above, "person acting on behalf of the Commission" includes any employee or contractor of the Commission, or employee of such contractor, to the extent that such employee or contractor of the Commission, or employee of such contractor prepares, disseminates, or provides access to, any information pursuant to his employment or contract with the Commission, or his employment with such contractor.

ORNL-4365

Contract No. W-7405-eng-26

UNIT OPERATIONS SECTION QUARTERLY PROGRESS REPORT

April-June 1968

CHEMICAL TECHNOLOGY DIVISION

M. E. Whatley

P. A. Haas
L. E. McNeese
A. D. Ryon
C. D. Watson

FEBRUARY 1970

OAK RIDGE NATIONAL LABORATORY
Oak Ridge, Tennessee
Operated by
UNION CARBIDE CORPORATION
for the
U. S. ATOMIC ENERGY COMMISSION

LOCKHEED MARTIN ENERGY RESEARCH LIBRARIES

3 4456 0515554 1

CONTENTS

Page

ABSTRACTS 1

1. BIOCHEMICAL SEPARATIONS 4
   1.1 Separation of Phenylalanine and Tyrosine tRNAs 4
   1.2 Separation of Methionine and Valine tRNAs 5

2. SOL-GEL DEVELOPMENT STUDIES 9
   2.1 Preparation of Urania Sols by Precipitation-Peptization 9
      2.1.1 Batch Preparation of UO_2 Sols by Precipitation 10
      2.1.2 Equipment for Continuous Preparation of UO_2 Sols by Precipitation 12
   2.2 Two-Fluid Nozzles Under Turbulent Flow Conditions as Sol Dispersers 14
   2.3 Preparation of UO_2-C Microspheres 17
   2.4 Gelation in Isoamyl Alcohol 18

3. MOLTEN-SALT REACTOR PROCESSING STUDIES 21
   3.1 MSRE Distillation Experiment 22
      3.1.1 Measurement of Distillation Rates 23
      3.1.2 Concentration Polarization and Entrainment . . 25
      3.1.3 Difficulties Encountered 30
      3.1.4 Postoperational Examination 31
      3.1.5 Conclusions 32
   3.2 Frozen-Wall Corrosion Protection 33
      3.2.1 Experimental Equipment and Procedures 35
      3.2.2 Experimental Results 37
   3.3 Studies of a Simulated Molten-Salt--Liquid-Bismuth Contactor 46
   3.4 Electrolytic-Cell Development 52

ABSTRACTS

1. BIOCHEMICAL SEPARATIONS

1.1 Separation of Phenylalanine and Tyrosine tRNAs

Continued processing to produce phenylalanine tRNA has yielded 2.3 x 10^6 picomoles of very pure material and 2.2 x 10^6 picomoles of phenylalanine tRNA contaminated with leucine tRNA. The high-purity material was obtained in the fractions associated with two peaks upon elution from the isopentyl acetate reversed-phase columns when fresh packing was used. Subsequent sorptions and elutions from the packing produced a product contaminated with leucine tRNA.

1.2 Separation of Methionine and Valine tRNAs

Excellent separations of formylmethionine 1 tRNA, formylmethionine 2 tRNA, and valine tRNA have been achieved in preliminary runs using an improved, scaled-up version of the earlier separation procedure. However, the success of the tests is tempered by the relatively low specific activity of the formylmethionine 1 tRNA. Attempts to explain this anomalous behavior are in progress.

2. SOL-GEL DEVELOPMENT STUDIES

The development of sol-gel processes for use in preparing ceramic nuclear fuels, particularly small UO_2 microspheres, was continued. UO_2 sols were prepared in batch precipitation-filtration-peptization equipment using a flowsheet featuring precipitation at pH 7.3. The development of equipment to allow UO_2 sols to be prepared by precipitation-washing-peptization, using a continuous type of operation, was terminated and summarized in a report. More than 10 liters of UO_2-C sol was formed into microspheres, using 2-ethyl-1-hexanol (2EH) temperatures of about 30 and 45°C to improve the operation. The method for preparing UO_2 spheres

smaller than 100 μ in diameter was improved by using a new sol-dispersion procedure and by using isoamyl alcohol in place of 2EH.

3. MOLTEN-SALT REACTOR PROCESSING STUDIES

A molten-salt breeder reactor (MSBR) will be fueled with a molten fluoride mixture that will circulate through the blanket and core regions of the reactor and through the primary heat exchanger. We are currently investigating several operations that may be used in a close-coupled processing facility for removing fission products, corrosion products, and fissile materials from the molten fluoride mixture; this facility will be an integral part of the reactor system.

3.1 MSRE Distillation Experiment

In a two-fluid MSBR, distillation may be used as a means for removing materials of low relative volatility (such as rare-earth fluorides) from an $LiF-BeF_2$ mixture, which is the fuel carrier salt for the reactor. In a single-fluid MSBR, distillation may be used for the partial recovery of lithium and beryllium fluorides from waste streams; it may also be used as a feed-adjustment step prior to other operations such as reductive extraction. The nonradioactive operation of a relatively large molten-salt distillation system was successfully demonstrated.

3.2 Frozen-Wall Corrosion Protection

We have concluded a series of experiments in which we simulated the heat-transfer and hydrodynamic characteristics of a continuous fluorinator. In these experiments, we demonstrated that a layer of frozen salt could be formed and maintained (on a test vessel) under conditions of flow and heat transfer approximately equivalent to those expected for processing fuel salt from a 1000-Mw (electrical) MSBR.

3.3 Studies of a Simulated Molten-Salt–Liquid Bismuth Contactor

The multistage contacting of molten salt with liquid bismuth containing lithium or thorium has been proposed for removing protactinium and rare-earth fission products from single-fluid MSBR's. A packed column in which this operation is simulated, using mercury and water, has been operated; some of the data are presented here. Additional measurements of flooding, dispersed-phase holdup, and pressure drop through the column are planned.

3.4 Electrolytic-Cell Development

We have designed and fabricated an electrolytic oxidation-reduction cell for producing a bismuth stream containing lithium or thorium, and for oxidizing such components as lithium, thorium, protactinium, uranium, and rare earths from a bismuth stream.

<u>Previous Reports in This Series for the Year 1968</u>

January-March	ORNL-4364

1. BIOCHEMICAL SEPARATIONS

C. W. Hancher H. O. Weeren

1.1 Separation of Phenylalanine and Tyrosine tRNAs

Using a small quantity of mixed tRNA (from E. coli, strain B) remaining from the processing runs of January and February 1967, we achieved our objective of demonstrating that improved techniques developed since the earlier processing runs are valid for operations on a larger scale. The processing steps consisted of: (1) sorption on, and elution from, a DEAE column, followed by the pooling of separate fractions rich in phenylalanine tRNA or tyrosine tRNA; (2) sorption of the products from the DEAE column on an isopentyl acetate reversed-phase column, and subsequent elution; (3) desalting of the resulting eluate on a gel column; and (4) concentration of the product from the gel column by evaporation. A fifth step--removal of high-molecular-weight contaminants by gel filtration--remains to be done.

During the preceding quarter all of the available mixed tRNA was processed on DEAE columns; four runs were made in which pooled fractions rich in phenylalanine tRNA were processed on isopentyl acetate reversed-phase columns. Three additional runs on the reversed-phase column were needed to process the remaining feed that was rich in phenylalanine tRNA; these runs were made during this report period. In three of the seven runs (i.e., the ones made with fresh packing), the phenylalanine tRNA was partially resolved into two peaks, whereas the second and third runs made on a given batch of packing had only one phenylalanine tRNA peak and the product was contaminated with leucine tRNA. In earlier production runs no such drastic deterioration of resolution with run number had been noted. The earlier runs were made using Chromosorb W packing, while the recent runs employed packing made from Chromosorb G. Whether or not this difference is significant is currently being investigated.

In the runs yielding two phenylalanine tRNA peaks, the product was divided into five fractions: (1) a forecut, (2) the first product peak, (3) an unresolved product cut (the material between the two peaks), (4) the second product peak, and (5) an aftercut. In runs yielding only one phenylalanine tRNA peak, the product was divided into three fractions: (1) a forecut, (2) the product peak, and (3) an aftercut.

Each product pool from the isopentyl acetate columns was desalted on a 4- by 84-in. Sephadex G-25 column at 5°C. The desalted pools were concentrated by evaporation, first in a wiped-film evaporator at 21°C and then in a rotary evaporator at 35°C. Each evaporator concentrate was treated with ethanol to precipitate the tRNA; the precipitated tRNA was separated by centrifugation and stored at -20°C.

The "first product peak" fraction from the binodal elution from the reversed-phase column (see Table 1.1) appears to be the best product. Its specific activity is high, and it contains no contaminating tRNAs. The quality of the other product pools from this elution appears to be almost as good. We believe that the specific activity of each of these product pools will improve by 10 to 20% when the pool is further processed, by gel filtration, to remove high-molecular-weight contaminants.

The DEAE product pools that were rich in tyrosine tRNA were processed in two runs on the reversed-phase column. The first run produced a tyrosine tRNA peak with a maximum specific activity of 730 picomoles/ODU. In the second run the tyrosine tRNA was not eluted in its usual position; instead, it was removed with the forecut. It was then precipitated with ethanol, centrifuged, redissolved in feed solution, and run again on the reversed-phase column. The specific activity of this product was only 200 picomoles/ODU. This experiment confirms the long-standing observation that the reversed-phase columns cannot be used for rechromatography.

1.2 Separation of Methionine and Valine tRNAs

In the phenylalanine tRNA production runs of January and February 1967, most of the tRNAs were eluted from the reversed-phase column very

Table 1.1. Results of Processing and Purifying Phenylalanine tRNA on Isopentyl Acetate Reversed- Phase Chromatographic Column

Fraction	Volume (ml)	Absorbance, A_{260} (ODU/ml)	Total Absorbance, A_{260} (ODU)	Specific Activity (picomoles/ODU)		Yield of Phenylalanine tRNA (picomoles)
				Phenylalanine tRNA	Leucine tRNA	
		Product with Two Phenylalanine tRNA Peaks				$x10^6$
Forecut	1250	0.150	187	855	0	0.16
First product peak	3250	0.240	780	1120	0	0.87
Unresolved product	1225	0.115	141	1060	0	0.15
Second product peak	3250	0.240	780	933	0	0.73
Aftercut	2800	0.178	500	740	0	0.37
						2.28
		Product with One Phenylalanine tRNA Product Peak				
Forecut	3280	0.265	870	408	142	0.35
Product peak	5200	0.410	2130	670	58	1.43
Aftercut	3625	0.230	830	530	81	0.44
						2.22

early in the run; they were subsequently precipitated with ethanol, centrifuged, and stored in the freezer. Recently we found that this material contained a considerable amount of methionine tRNA (7200 mg) and that about 60% of this methionine tRNA, along with appreciable amounts of valine tRNA, could be separated from the other tRNAs. This separation is made on an RPC-3 column, namely, a column of diatomaceous earth coated with trioctylpropylammonium bromide. When the early-eluted tRNAs are loaded onto this column and then eluted with a gradient solution of sodium chloride, the first tRNAs to be eluted occur in two methionine tRNA peaks and a valine tRNA peak. The methionine in both peaks is formyl accepting; these peaks are, therefore, designated as formylmethionine 1 tRNA, or $tRNA_1^{fMet}$, and formylmethionine 2 tRNA, or $tRNA_2^{fMet}$.

The relative amount of methionine tRNA in the early-eluted material can be increased threefold by processing on a DEAE cellulose column. Thus about 85% of the early-eluted material was processed either on a 4-in. DEAE column (eight runs) or a 2-in. DEAE column (five runs). The fractions rich in methionine tRNA were pooled, precipitated with ethanol, centrifuged, and frozen. The non-methionine fraction was similarly treated. The overall loss of methionine tRNA was 10%; another 10% of the methionine tRNA was pooled with the non-methionine tRNA fraction.

Many runs using 2-in. RPC-3 columns have been made in Chemical Development Section A. Scale-up of these runs in the Unit Operations Section to a 4-in. column is now in progress. In the first runs on the 4-in. column, excellent separation of the $tRNA_1^{fMet}$ from the $tRNA_2^{fMet}$ was achieved. The separation of valine tRNA from $tRNA_1^{fMet}$ was equivalent to that achieved on the 2-in. column. Hence, direct scale-up from the 2-in. column to the 4-in. column appears feasible.

The one disappointing feature of the runs made on the 4-in. column was the somewhat lower specific activity of the $tRNA_1^{fMet}$ peak. Test runs made on a 2-in. RPC-3 column in our laboratory produced a peak for $tRNA_1^{fMet}$ with a specific activity even lower (by about 10 to 20%) than that observed earlier in Chemical Development Section A. This lower

specific activity seems common to all runs made in the Unit Operations Section, and does not appear to be related to scale-up. Parallel runs are now in progress in the Unit Operations and the Chemical Development Sections to attempt to isolate the cause of the differences in specific activity.

2. SOL-GEL DEVELOPMENT STUDIES

P. A. Haas

The objective of these studies is to develop optimum sol-gel processes for the preparation of ceramic fuels containing uranium, plutonium, thorium, and their mixtures. The present emphasis is on preparing urania or urania-thoria sols and, subsequently, using these sols to produce oxide microspheres.

Each of the several flowsheets that have been developed for preparing UO_2 sols starts with uranyl nitrate solution and involves the following conversions:

1. Reduction of uranyl nitrate to uranous nitrate by hydrogen in the presence of a catalyst.
2. Formation of a hydrated uranous oxide.
3. Removal of nitrate and other anions or cations.
4. Dispersion of the hydrated uranous hydroxide as colloidal crystallites.

The suitability of the resulting sols for use in the production of UO_2 microspheres is dependent on the sol-preparation conditions and on the operating conditions in the sphere-forming column.

2.1 Preparation of Urania Sols by Precipitation-Peptization

P. A. Haas

Batch precipitation-washing-peptization processes were the first successful methods for preparing UO_2 sols at Oak Ridge National Laboratory. These processes have been used to prepare a large number of enriched-, natural-, and depleted-uranium sols. Also, sol-gel products to be used for irradiation tests or other purposes have been prepared by batch precipitation procedures. However, because of criticality problems and the number of operating steps inherent in the batch flowsheets, continuous-

type equipment is preferred for large-scale remote operation. The engineering development of such equipment for preparing UO_2 sols by precipitation-washing-peptization has been completed and described in a summary report.[1] All of the flowsheets for preparing UO_2 sols by precipitation require the same principal operations:

(1) Reduction of uranyl nitrate to uranous nitrate by hydrogen in the presence of a catalyst.

(2) Precipitation of uranous hydroxide by ammonia.

(3) Washing of the precipitate to remove NH_4NO_3, NH_4OH, and other solutes.

(4) Dispersion with NO_3^-.

2.1.1 Batch Preparation of UO_2 Sols by Precipitation

We are continuing to prepare UO_2 sols, using normal uranium, in the batch PFP (Precipitation-Filtration-Peptization) vessel. Precipitation, washing, and dispersion are done in this vessel, which has a 12-in.-diam, porous, stainless steel plate as the bottom and contains a slow-speed, paddle type agitator. Supernates (present after precipitation and after each of four washing steps) are removed by filtration and decantation. Washing is accomplished by contacting the 5 liters of slurry or cake remaining on the filter with 10 liters of water. The precipitate is peptized by agitation and heating after the addition of HNO_3.

The current flowsheet for preparing sols in the PFP vessel features precipitation at a pH of 7.3 (Fig. 2.1). This flowsheet also includes the step in which U(IV) nitrate solution is prepared in a fixed-bed reactor; however, we would use this same flowsheet (starting with the precipitation step) even if the U(IV) were prepared in another type of reduction reactor. When the precipitate is stirred during the washing step, a sufficient amount of nitrate ion must be removed so that the washed precipitates will settle satisfactorily and will not partially deflocculate; the presence of

---

[1] P. A. Haas, Engineering Development of Continuous Sol-Gel Equipment for Preparing UO_2 Sols by Precipitation-Peptization Processes, ORNL-TM-2227 (July 1968).

ORNL DWG 68-802-R3

BASIS: CONCENTRATIONS OR AMOUNTS OF U(IV), NO_3^-, HCOOH, OR NH_4^+ ARE IN MOLES/MOLE U.

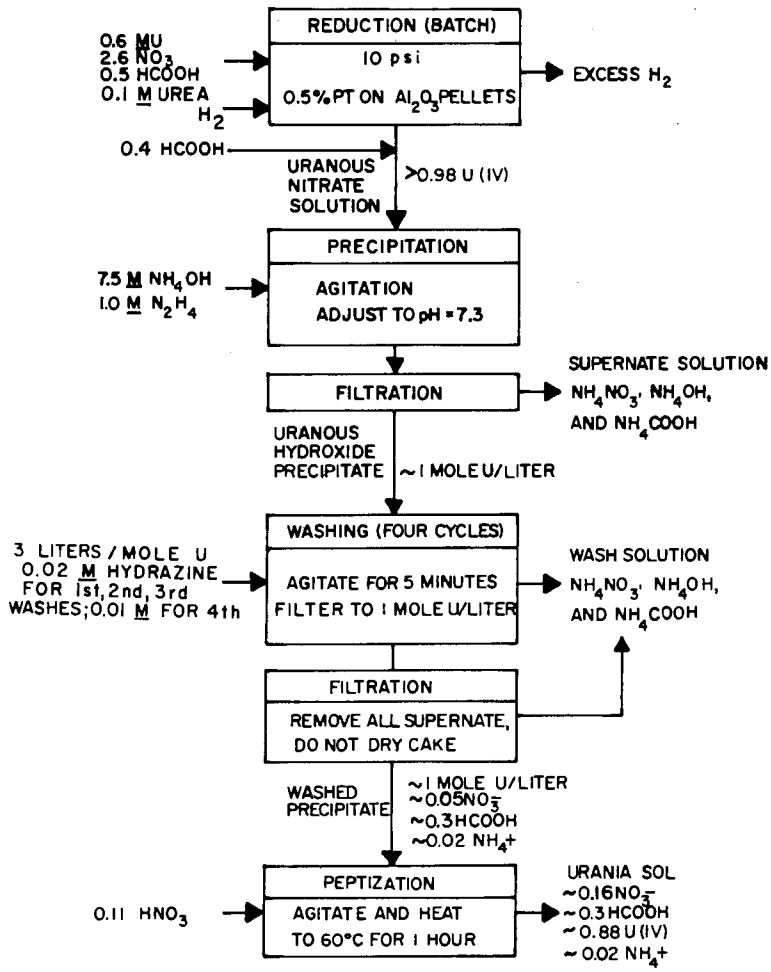

Fig. 2.1. Batch Precipitation-Filtration-Peptization (PFP) Preparation of Urania Sol.

hydrazine in the wash water (Fig. 2.1) promotes the removal of nitrate ion. The lower pH used in this flowsheet (as compared with that used previously) appears to give a more dispersible precipitate and a more stable, and less thixotropic, sol. Sols prepared under these conditions (Table 2.1) have remained fluid until used (up to three months), and have yielded good-quality UO_2 spheres.

The first batch of U(IV) nitrate solution prepared in the fixed-bed reduction reactor after a shutdown of a week or longer produces a sol having anomalous characteristics. The precipitate is slower in settling and has lower settled densities in the PFP vessel, while the product sol has lower uranium concentrations and $HCOO^-/U$ mole ratios (see Table 2.1) and is more thixotropic. Even a two-day shutdown shows some effect; for example, there are noticeable differences between sol F-107 [U(IV) reduction done May 24, 1968] and sol F-108 [U(IV) reduction done May 27, 1968]. Sols F-103 through F-110 were produced during the most routine operation of this equipment. One individual prepared the eight batches (about 10 kg of UO_2, total) over a period of nine days. These sols are now being used to form PuO_2-UO_2 microspheres and PuO_2-UO_2 gel shards, and for UO_2 extrusion studies. The uranium concentrations of these sols are higher than those of any fluid sols previously prepared by using this system.

2.1.2 Equipment for Continuous Preparation of UO_2 Sols by Precipitation

Since these studies have been terminated and summarized in a report, only the conclusions and recommendations from the report[1] will be presented here.

> "Continuous equipment can be used to prepare UO_2 sols by precipitation-washing-peptization flowsheets. When mechanical operation is good, the continuous systems give sols of the desired chemical compositions and good visual appearance. However, these sols (particularly those from the continuous vacuum evaporator) are not identical to those from batch equipment. The characteristics of the sols and the conditions to form them into UO_2 microspheres require further study.
>
> "The major problems were with respect to mechanical operability and dependability, with the transfer of precipitate as the major source of operating difficulty. By increasing the pipe sizes to 1/2 inch diam minimum and limiting the slurry concentrations to 50 g U/ℓ or less, the operation of acid-egg type pumps between washer stages was improved to marginal acceptability. When the requirements for remote operation are considered, there are minor mechanical operating problems without obvious solutions. These would probably always be sources of difficulty, but could be tolerated if no alternatives were

Table 2.1. Analyses of Batch Agitated-Filter Urania Sols

Uranous nitrate with NO_3^-/U and $HCOO^-/U$ ratios of 2.6 and ~ 0.7, respectively. Fixed-bed reduction of U(VI) to U(IV) except for runs F-90 through F-93 in which slurry catalyst was used.

Identification No.	Date Prepared	Uranium Conc. (M)	Mole (or Atom) Ratios U(IV)/U	NO_3^-/U	C/U	NH_4^+/U	X-ray Crystallite Size (111) (A)
F-90	1-22-68	1.07	0.92	0.174	0.63	0.032	55
F-91	1-23-68	0.76	0.90	0.168	0.49	0.025	57
F-92	3-7-68	0.85	0.89	0.147	0.33	0.018	--
F-93	3-8-68	0.59	0.87	0.155	0.39	0.029	--
F-94	4-5-68	Would Not Peptize					
F-95	4-9-68	0.78	0.89	0.170	0.39	0.022	61
F-96	4-10-68	0.84	0.90	0.160	0.42	0.020	64
F-97	4-11-68	1.11	0.90	0.130	0.40	0.017	--
F-98	4-30-68	0.63	0.86	0.170	0.23	0.030	64
F-99	5-7-68	0.69	0.88	0.149	0.24	0.013	60
F-100	5-8-68	1.05	0.90	0.160	0.37	0.016	66
F-101	5-9-68	1.06	0.90	0.155	0.38	0.016	70
F-102	5-10-68	1.00	0.89	0.140	0.39	0.019	--
F-103	5-21-68	0.63	0.88	0.163	0.25	--	--
F-104	5-22-68	1.07	0.90	0.153	0.37	--	--
F-105	5-23-68	1.19	0.90	0.141	0.33	--	--
F-106	5-24-68	1.27	0.89	0.156	0.40	--	--
F-107	5-27-68	1.26	0.90	0.150	0.39	--	--
F-108	5-28-68	1.02	0.89	0.133	0.29	--	--
F-109	5-29-68	1.29	0.90	0.136	0.42	--	--
F-110	5-30-68	1.41	0.90	0.134	0.45	--	--

available. The preparation of UO_2 sol by solvent extraction as reported elsewhere has very few mechanical problems.

"The principal conclusions with respect to individual operations were:

1. The continuous, high-pressure reduction system adequately met the chemical flowsheet requirements. The low-pressure reduction procedures recently developed are now preferred and the high-pressure reduction flowsheets are obsolete.
2. The continuous precipitators, as revised, operate without difficulty other than those from feed metering problems.
3. The precipitation can be controlled by metered flows, but pH indicators in the slurry are not dependable.
4. Washing is excellent in the stage washers with stage efficiencies of about 80%, but the transfer of precipitate between stages is still of marginal acceptability.
5. Washing in a countercurrent column gives HTU values of 2.3 to 3.6 feet. Fifteen to twenty feet of column would be desirable to give good washing although twelve feet gave acceptable washing for most tests.
6. Settling of the washed precipitate to give a uranium concentration of more than 0.5 M in the sol is not practical.
7. The continuous peptizers give adequate dispersion with no clear chemical advantages or disadvantages if the slurry, HNO_3, and HCOOH flow rates are controlled.
8. We do not have an adequate pump to meter washed precipitate from the washer into the peptizer system.
9. The use of a vacuum evaporator for concentrating UO_2 sols has been adequately demonstrated in other sol preparation studies.
10. The chemical flowsheet conditions have much more effect on the sol characteristics than does the choice of continuous or batch flowsheet.
11. The sols from the continuous preparation equipment (particularly those from the continuous vacuum evaporator) are not identical to those from batch equipment. Their characteristics and the conditions required to form them into UO_2 microspheres require further study."[1]

2.2 Two-Fluid Nozzles Under Turbulent Flow Conditions as Sol Dispersers

P. A. Haas S. D. Clinton

We are continuing to use two-fluid nozzles with organic flow rates that are too high to allow the varicose type of dispersion that we use for large sol drops. We call this type of dispersion "turbulent two-fluid

nozzle" dispersion. However, we have found that the varicose mechanism disappears at Reynolds numbers for the organic drive fluid between 500 and 1000, although true turbulence throughout the flow channel does not occur until the Reynolds number approaches 2000. In the intermediate region, there is a combination of shear and promoted turbulence, which is useful for obtaining sol drops with mean diameters of 50 to 300 μ. A sharp discontinuity in the mean drop diameter and in the uniformity of the drop size occurs for a small change in flow rate at the point where the varicose mechanism changes to "turbulent" flow. Once this transition point is passed, the uniformity of drop size remains approximately constant and the mean size decreases continuously as the Reynolds number is increased. The sol drop size appears to depend principally on the viscosity and flow rate of the organic drive fluid, and on the nozzle diameter. The sol flow rate, sol properties, and other nozzle dimensions are much less important.

The two-fluid nozzle with the sol inlet capillary located perpendicular to the tube axis is the preferred arrangement for preparing small microspheres. This disperser design, which we have designated the "turbulent two-fluid nozzle," has several important advantages even though the uniformity of drop size obtained near the mean size is not significantly better than for other dispersers we have tested. These advantages are:

(1) The number of extremely small spheres is greatly diminished. The presence of such small spheres (with diameters smaller than 0.2 times the mean diameter) greatly increases sintering and clumping during the drying and firing. These small spheres are the chief cause of entrainment and losses. They tend to attach themselves to larger spheres and are difficult to separate during sieving.

(2) The mean size of the spheres can be varied by simply varying the flow rates.

(3) The results are reproducible and are independent of the system configuration outside the nozzle.

(4) The mean drop diameter can be varied from about 300 μ to less than 30 μ (or from about 90-μ to less than 10-μ product for a UO_2 sol).

The two-fluid nozzle design with the axial sol inlet, as we normally use it for streamline or varicose operation, is less suitable for "turbulent" operation. The actual turbulent mechanism for the larger drops below the varicose range (i.e., from 300-μ to about 100-μ drops) is a combination of shear and promoted turbulence, and the perpendicular sol inlet is more effective than the axial inlet. The small annulus around the axial sol inlet causes a high pressure drop, which limits the maximum organic flow rate, and thus the minimum drop size, possible. A larger annulus would require much higher total flow rates of organic, although the pressure drops would be less. The perpendicular sol inlet avoids the flow restriction and hence, for a given inside diameter and organic flow rate, gives a lower pressure drop than the axial sol inlet, thus allowing the formation of smaller drops without requiring excessive pressures.

Recent results obtained by using the turbulent two-fluid nozzle dispersers show that about 60 wt % of the product is generally between 0.7 and 1.4 d_{50}, where d_{50} is the mean diameter. The weight distribution gives a straight line on log-probability paper. The sol drop diameter for nozzles approximately 2 mm in inside diameter can be estimated from:

$$D_{sol} = 10^6 \frac{\mu^{1.5}(ID)^{1.0}}{G^{1.5}},$$

where

D_{sol} = mean sol drop diameter (μ),
μ = organic viscosity (cp),
ID = inside diameter of nozzle (cm),
G = organic flow rate (cc/min).

This equation was derived by using a small number of measurements, and is, therefore, intended only for use in cases in which the variations from the experimental conditions tested are minimal. Although its absolute accuracy

is not high, the equation can be useful in correcting for temperature variations or in calculating the change in flow rate to give a desired change in D_{sol}.

2.3 Preparation of UO_2-C Microspheres

P. A. Haas S. D. Clinton
R. E. Norman*

About 6 liters of UO_2-C sol that had been prepared from UO_2 sols F-92 and F-97 (Table 2.1) were formed into gel microspheres about 175 μ in mean diameter. By increasing the column temperature to about 43°C, the gel spheres were formed without difficulty using Span 80 as the only surfactant in the 2EH. In a previous test with a similar UO_2-C sol, six additives were included and the temperature was increased before clustering and sticking became tolerable; apparently the increased temperature was the most effective change for decreasing the clustering of the sol containing carbon.

About 4 liters of UO_2-C sol that was formed by adding carbon** to sols F-102 and F-104 (Table 2.1) yielded good-quality gel spheres, using 2EH at about 30°C, 0.1 vol % Span 80, and about 1.5 vol % H_2O in the 2EH. The shapes of the gel particles were distorted when higher surfactant concentrations, higher temperatures, or lower water concentrations were used. Interestingly, sols F-102 and -104 without added carbon did not give distorted particles at the higher surfactant concentrations or lower water contents.

In general, the addition of carbon to UO_2 sols made the formation of gel spheres more difficult. The higher-quality UO_2-C sols required lower surfactant concentrations (in agreement with the results obtained for UO_2 sols containing no carbon). Apparently, the sols that are charac-

---

*Employee of Gulf General Atomic.

**Carbon added by Chemical Development Section A.

terized by excellent fluidity and stability are farther from gelation and require slower extraction of water and lower surfactant concentrations to avoid distortion during gelation.

2.4 Gelation in Isoamyl Alcohol

P. A. Haas S. D. Clinton

A simple system was installed and operated for preparing small gel spheres (< 100 μ in diameter) without fluidization. This system was designed to take advantage of the easier separation of gel spheres and the more rapid gelation that are possible with isoamyl alcohol [as compared with 2-ethyl-1-hexanol (2EH)].[2] It uses one pump and one settler-surge tank (Fig. 2.2). The 18-in.-diam cone-bottom tank has a much larger volume than an inclined-slab settler of the same efficiency. The open-top design was selected to provide a large organic surface for use in tests of dispersion devices and also to act as a surge vessel. The lower boiling point and higher water content possible in isoamyl alcohol, as compared with 2EH, allow the use of low-pressure (20-psig) steam, lower organic flow rates to the still, and smaller heat exchangers.

The system was initially operated with a baffled, agitated, 4-liter vessel as the dispersion-gelation apparatus; however, most of the operation involved the use of a turbulent two-fluid nozzle and associated standpipe. (The turbulent two-fluid nozzle is discussed in Sect. 2.2.) The still was initially supplied with low-pressure steam (nominally 15 psig). The temperature of the still allowed a water content of more than 5.0 vol % in the isoamyl alcohol during normal operation. Clustering and sticking were considerably alleviated, and gelation was more rapid when a 21-psig steam supply was used to keep the water content below this value.

In the system shown in Fig. 2.2, 21-psig steam was supplied to the still, and essentially no surfactant was added to the isoamyl alcohol.

---

[2] M. E. Whatley *et al.*, Unit Operations Section Quarterly Progress Report, October-December 1967, ORNL-4235.

ORNL DWG 68-7661

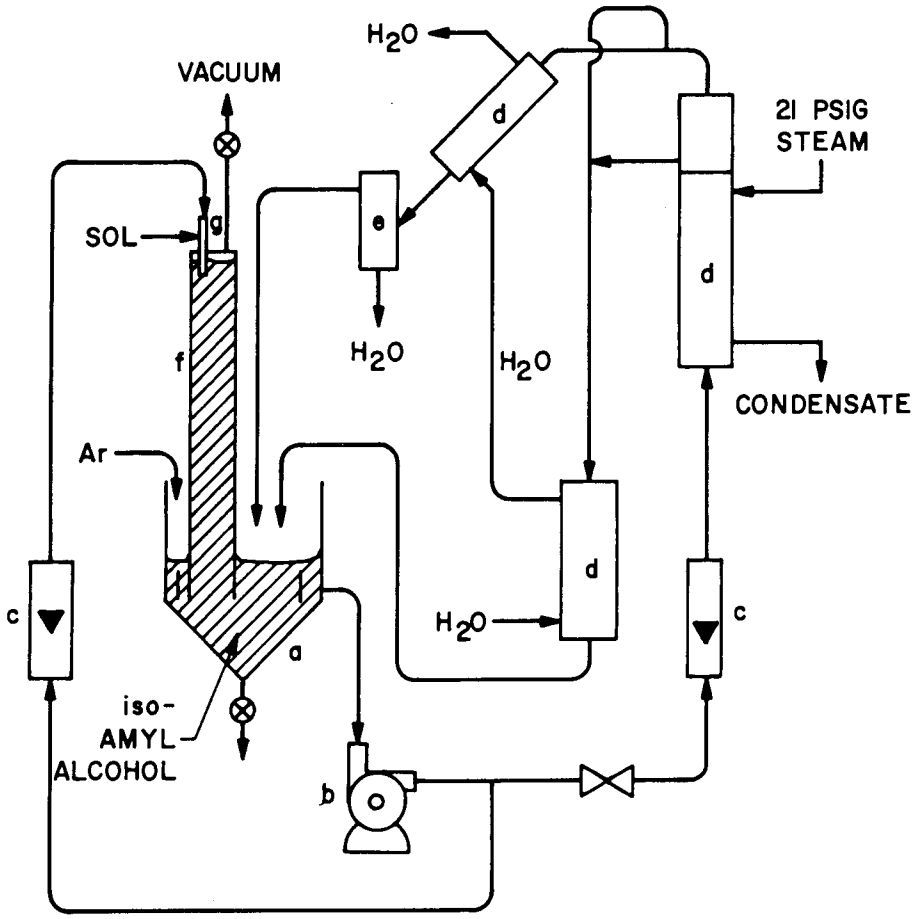

a. SETTLER-SURGE TANK
b. CENTRIFUGAL PUMP
c. ROTAMETERS
d. HEAT EXCHANGERS
e. PHASE SEPARATOR
f. METHACRYLATE PLASTIC PIPE, 3.5 in. ID
g. TWO—FLUID NOZZLE

Fig. 2.2. Settler-Still System for the Preparation of Small Gel Spheres, Using Isoamyl Alcohol as the Organic Liquid.

However, with a lower steam pressure and the resulting water content (above 5 vol%) in the alcohol, the addition of surfactants was necessary to prevent clustering and sticking. The preparation of -325-mesh ThO_2 spheres required the addition of Ethomeen S/15 every 30 min. UO_2 spheres were prepared in alcohol containing 0.1 to 1.0 vol % Span 80. The plastic standpipe shown in Fig. 2.2 eliminated, to some extent, the sticking that occurred during operation with UO_2 sol and low-pressure steam. When 21-psig steam was used, UO_2, UO_2-C, and other sols gave no significant sticking or clustering problems in isoamyl alcohol containing no surfactants. We have not yet studied ThO_2 sols under these conditions. The addition of surfactants may still be desirable in order to obtain spheres with smooth surfaces.

In summary, the use of isoamyl alcohol provides more rapid gelation and more rapid or easier settling of the product. Also, isoamyl alcohol is easier to remove from the gel than is 2EH. It appears to be easier to obtain small-diameter spheres with low carbon contents and high densities when isoamyl alcohol, rather than 2EH, is used although the experimental data suggesting this are not conclusive. With some sols, isoamyl alcohol yields distorted particles whereas 2EH yields good-quality spheres. Both alcohols give a good-quality product in the case of very small UO_2 microspheres. The properties of -325-mesh UO_2 spheres prepared in isoamyl alcohol (Table 2.2) are more desirable than those for -325-mesh UO_2 spheres prepared in 2EH.

Table 2.2. Analyses for -325-Mesh UO_2 Spheres Prepared in Isoamyl Alcohol

Sample	UO_2 Sol[a]	Carbon Content (ppm)	O/U Atom Ratio	Surface Area (m^2/g)	Density (g/cc)
2-28-1317	F-87	< 20	---	0.029	10.88
3-19-1600	EV-19	340	---	0.070	10.55
4-23-1615	F-92	30	2.0049	---	10.39
4-23-1615	F-92	40	2.0044	---	10.41
6-6-1410	F-103	30	2.0144	0.065	10.26

[a]All sols were prepared by precipitation except EV-19, which was prepared by solvent extraction.

3. MOLTEN-SALT REACTOR PROCESSING STUDIES

L. E. McNeese

A molten-salt breeder reactor (MSBR) will be fueled with a molten fluoride mixture that will circulate through the blanket and core regions and through the primary heat exchanger. A close-coupled processing facility for the removal of fission products, corrosion products, and fissile materials from the molten fluoride mixture will be an integral part of the reactor system.

Several operations under study may be used in MSBR processing. The first, distillation, was initially considered as a means for removing materials of low volatility (such as rare-earth fluorides) from a $LiF-BeF_2$ mixture, which is the fuel-carrier salt of a two-fluid MSBR. This approach is not feasible for single-fluid MSBR's, since the salt stream of a single-fluid MSBR also contains the relatively nonvolatile ThF_4. Distillation may be important, however, for partial recovery of LiF and BeF_2 from waste streams, and it may be used as a feed-adjustment step prior to other operations such as reductive extraction. We have successfully demonstrated the nonradioactive operation of a relatively large molten-salt distillation system.

Fluorination of a molten-salt stream for uranium removal is another potential step in MSBR processing. Corrosion is an important problem associated with this operation, especially since there is considerable incentive for operating the fluorinator in a continuous manner. We have studied a system that allows simulation of the heat transfer and hydrodynamic characteristics of a continuous fluorinator having frozen-wall protection.

The proposed method for removing protactinium and rare-earth fission products from single-fluid MSBR's is reductive extraction, which involves the countercurrent contact of molten salt and liquid bismuth containing lithium or thorium in multistage contactors. Equipment that will permit

simulation of a salt-metal packed-column contactor using mercury and water has been assembled; it will allow us to make measurements of flooding, dispersed-phase holdup, and pressure drop through a packed column.

An electrolytic oxidation-reduction cell for producing bismuth containing lithium or thorium and for oxidizing components such as lithium, thorium, protactinium, uranium, and rare earths from a bismuth stream has been designed and fabricated.

3.1 MSRE Distillation Experiment

J. R. Hightower L. E. McNeese

Low-pressure distillation may be a key step in processing the fuel salt of molten-salt breeder reactors (MSBRs), either by direct removal of slightly volatile lanthanide fission products or by producing salt streams with compositions suitable for treatment by reductive extraction. Equipment has been designed and built to demonstrate low-pressure distillation of a batch of irradiated fuel salt from the MSRE. This equipment, described previously,[3] was extensively tested with nonradioactive material before being moved to the MSRE site for operation with actual fuel salt. The purposes of these tests were: (1) to determine the suitability of the equipment for radioactive operation and to gain operating experience, (2) to measure vaporization rates in large equipment, (3) to measure the extent of concentration polarization and/or entrainment, and (4) to uncover unexpected areas of difficulty in operation.

The first phase of the MSRE distillation experiment was performed in Building 3541, which is specially equipped for experiments involving large quantities of beryllium. Installation of the equipment began on September 1, 1967, and the first 48-liter batch of salt was introduced into the system on December 14, 1967. The nonradioactive operation was completed June 18, 1968. During the 187 days of operation, six batches of

---

[3] M. E. Whatley *et al.*, *Unit Operations Section Quarterly Progress Report, October-December 1967*, ORNL-4235.

salt were processed in the equipment. The six runs are summarized in Table 3.1.

During 185 days of this operation, the feed tank, the receiver, and the lower zones of the condenser were maintained at 550-600°C. The still-pot was at various temperatures for various lengths of times as indicated below:

Temperature (°C)	Period of Time
~ 25	12 days
500-650	56 days
750-875	110 days
900-1000	100 hr
1000-1005	160 hr
1005-1025	45 hr

3.1.1 Measurement of Distillation Rates

Distillation rates were determined by observing the rate of rise of liquid level in the condensate receiver. The rate measurements and the operating conditions are given in Table 3.2.

Table 3.2. Summary of Rate Measurements

Run No.	Temperature of Still (°C)	Condenser Pressure (mm Hg)	Distillation Rate ($ft^3\ ft^{-2}\ day^{-1}$)
MSS-C-1	990	0.5	1.15
MSS-C-1	990	0.3	1.20
MSS-C-1	990	0.055	1.25
MSS-C-2	1005	0.07	1.50
MSS-C-3	1004	0.075	1.56
MSS-C-4	1020	0.065[a]	1.63
MSS-C-5	950	0.08	0.66
MSS-C-5	1000	0.08	1.21
MSS-C-5	1025	0.08	1.95
MSS-C-6	1000	0.08	1.40

[a] This may not be the actual condenser pressure since a ZrF_4 plug occurred in the vacuum line during this run.

Table 3.1. Summary of Nonradioactive Experiments with Molten-Salt Still

Run No.	Dates	Conditions: Still Temp. (°C)	Conditions: Condenser Pressure (mm Hg)	Feed Material	Vol. Salt Distilled (liters)	Time Required (hr)	Purpose	Remarks
MSS-C-1	2/5/68 to 2/9/68	990	0.06-0.5	$LiF-BeF_2-ZrF_4$ (65-30-5 mole %)	35	83	To gain operating experience and to see effect of condenser pressure on vaporization rate.	
MSS-C-2	2/26/68 to 2/28/68	1005	0.07	$LiF-BeF_2-ZrF_4$ (65-30-5 mole %)	32	40	Same as MSS-C-1.	Metallic deposit restricted salt feed line.
MSS-C-3	3/26/68 to 3/27/68	1004	0.075	$LiF-BeF_2-ZrF_4-NdF_3$ (65-30-5-0.3 mole %)	26.4	31	To investigate polarization and entrainment.	
MSS-C-4	4/8/68 to 4/10/68	980-1020	0.065	Distilled salt from MSS-C-1	28	45	To see the effect of temperature on vaporization rate.	ZrF_4 condensation in vacuum line resulted in abnormally low rates.
MSS-C-5	5/27/68 to 5/28/68	950-1025	0.08	$LiF-BeF_2-ZrF_4-NdF_3$ (65-30-5-0.3 mole %)	32	41	To see the effect of temperature on vaporization rate.	
MSS-C-6	6/11/68 to 6/13/68	1000	0.08	$LiF-BeF_2-ZrF_4-NdF_3$ (65-30-5-0.3 mole %)	32	53	To see if polarization becomes evident after long operating times.	ZrF_4 condensation in vacuum line stopped distillation. Heating the line to 950-1050°C removed the obstruction.

The data in this table show that the distillation rate increased when the condenser pressure was lowered or when the still-pot temperature was raised. Figure 3.1 shows the effect of still-pot temperature on the vaporization rate for the runs in which the condenser pressure was below 0.1 mm Hg. A vaporization surface area of 10 ft^2 would be required for a still having a throughput of 15 ft^3/day and a still-pot temperature of 1000°C. A still of this size is considered to be feasible.

3.1.2 Concentration Polarization and Entrainment

The degree of separation of slightly volatile lanthanide fluorides from the feed salt can be seriously impaired by entrainment of liquid from the still or by a buildup of these less-volatile materials at the liquid-vapor interface (concentration polarization). The extent of this impairment can be inferred from the variation in the ratio of the NdF_3 concentration in the distillate to the average NdF_3 concentration in the still-pot liquid; this ratio will be denoted by R. If the effects of concentration polarization or entrainment are negligible, R will remain constant and will be equal to the relative volatility of NdF_3 with respect to LiF. The relative volatility of NdF_3 with respect to LiF, denoted by $\alpha_{NdF_3\text{-}LiF}$, has a value[4] of 1.4×10^{-4}. If either entrainment or concentration polarization occurs, R will be greater than $\alpha_{NdF_3\text{-}LiF}$. For example, if 0.1% of the condensate consisted of entrained still-pot material, R would be an order of magnitude greater than the relative volatility.

The effect that concentration polarization would have if it had occurred is indicated by the smooth curves in Figs. 3.2-3.4. The ratio R is seen to depend on the dimensionless expression $(\frac{D}{vL})$, which qualitatively represents the ratio of the rate of diffusion of the slightly volatile material from the interface to the rate at which material is carried to the interface by liquid moving toward the vaporization surface. (In the dimensionless expression, D is the effective diffusivity, v is the velocity of

[4] J. R. Hightower, Jr., and L. E. McNeese, Measurement of the Relative Volatilities of Fluorides of Ce, La, Pr, Nd, Sm, Eu, Ba, Sr, Y, and Zr in Mixtures of LiF and BeF_2, ORNL-TM-2058 (January 1968).

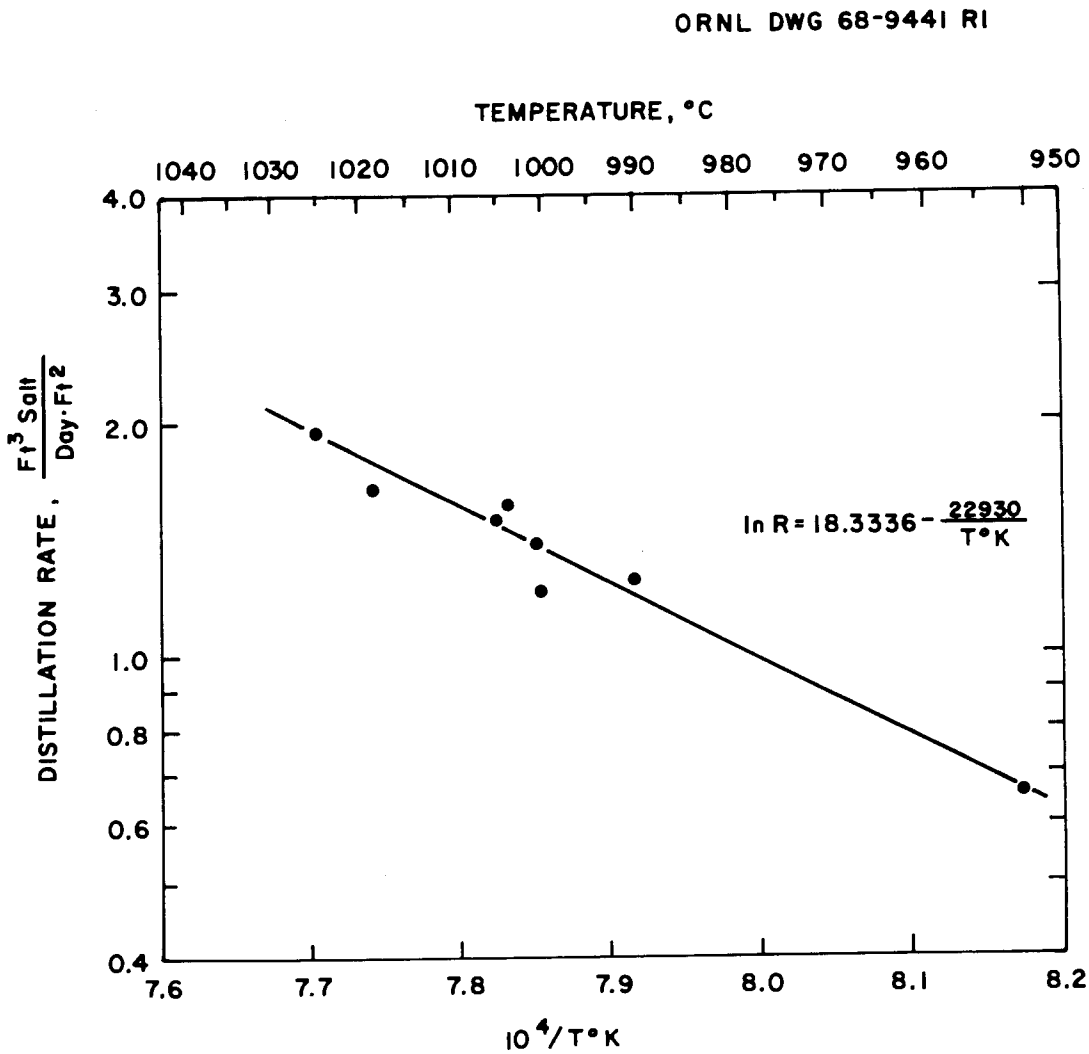

Fig. 3.1. Variation of Distillation Rate with Temperature at Low Condenser Pressure (0.05 - 0.09 mm Hg).

ORNL DWG. 69-10408

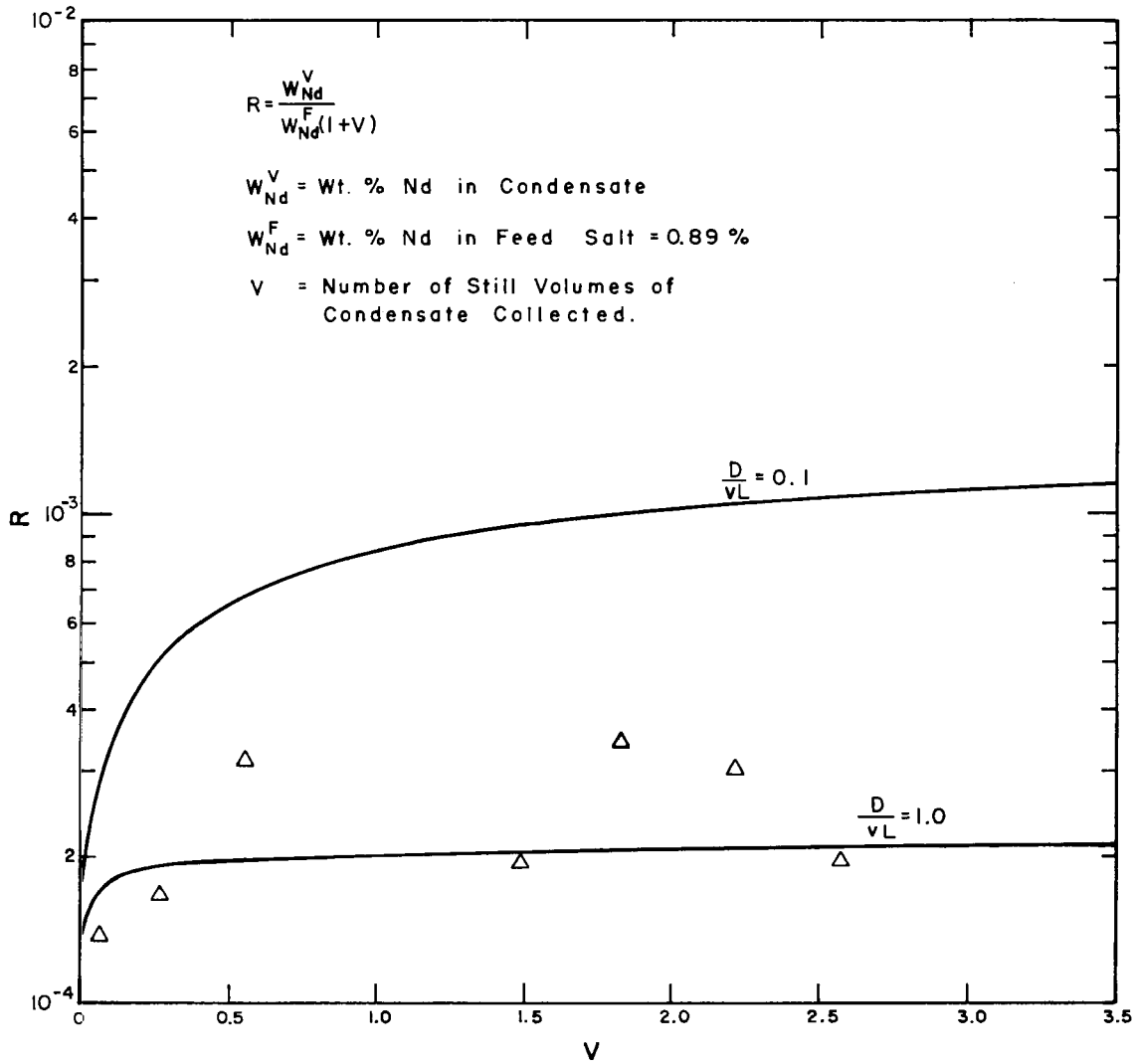

Fig. 3.2. Ratio of Neodymium in Condensate to Neodymium in Still Liquid for Run MSS-C-3.

ORNL DWG. 69-10412

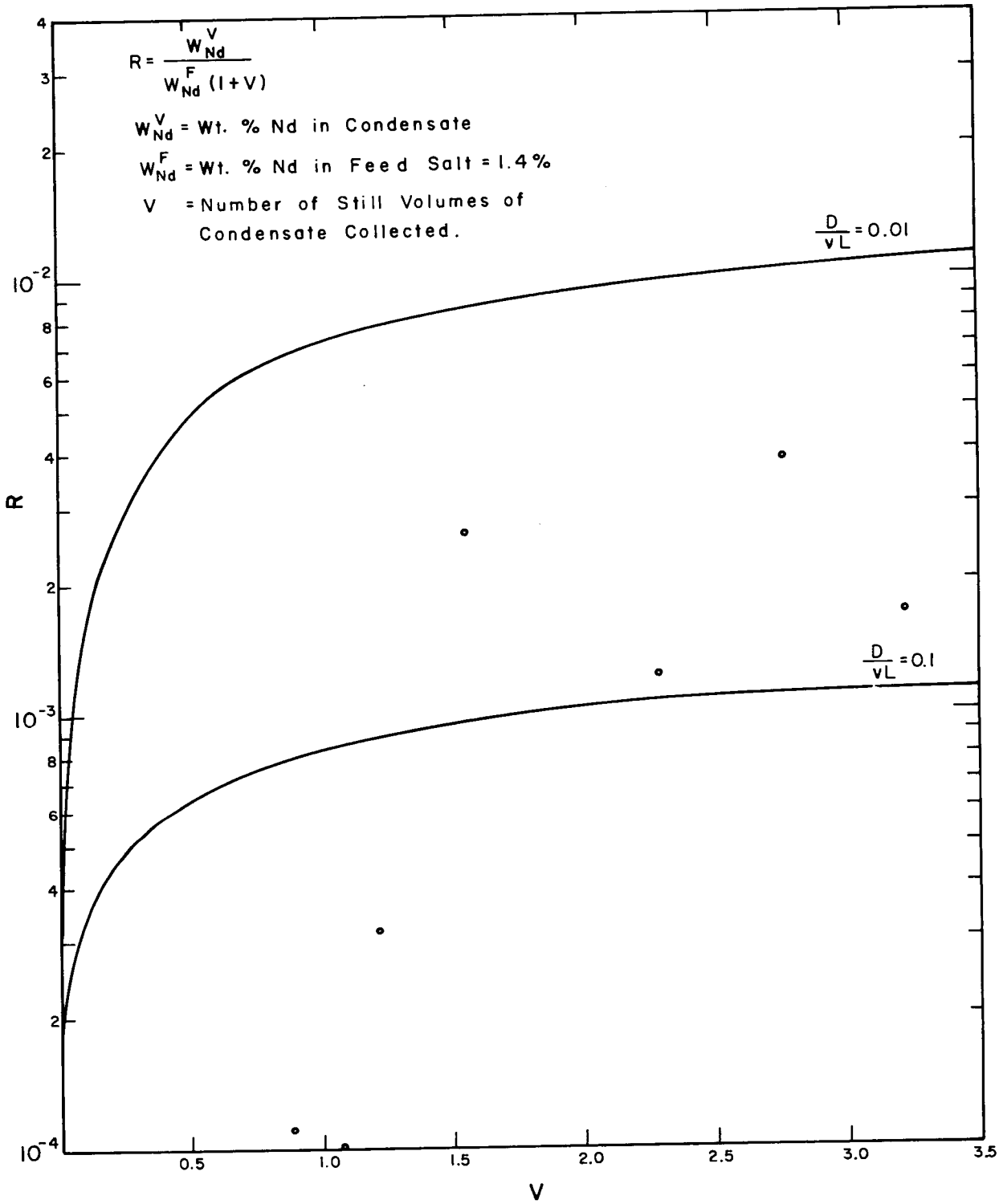

Fig. 3.3. Ratio of Neodymium in Condensate to Neodymium in Still Liquid for Run MSS-C-5.

ORNL DWG. 69-10410

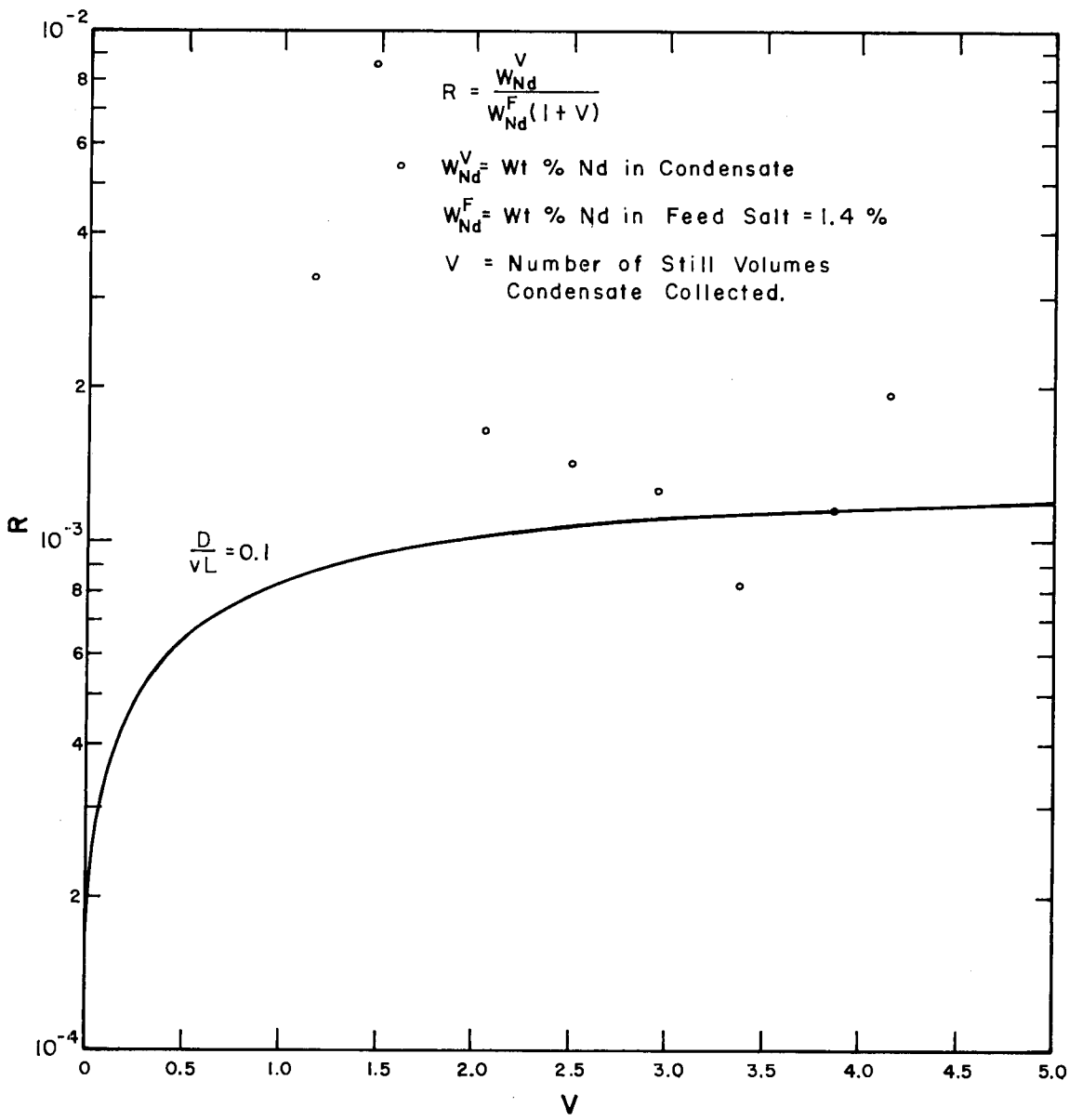

Fig. 3.4. Ratio of Neodymium in Condensate to Neodymium in Still Liquid for Run MSS-C-6.

liquid moving to the interface, and L is the distance between the vaporization surface and the point at which the feed salt is introduced.) The method used in calculating the curves in Figs. 3.2-3.4 is given in ref. 5.

Although the measurements of the NdF_3 concentration in the condensate do not enable one to distinguish between entrainment and polarization, they do indicate whether either effect is serious. In run MSS-C-3 (Fig. 3.2), polarization and/or entrainment was not serious since R consistently remained near 1.4×10^{-4}. In runs MSS-C-5 and MSS-C-6 (Figs. 3.3 and 3.4), substantially higher values for R were obtained. However, liquid having a high NdF_3 concentration had remained in the sample reservoir and on the condenser walls after the still pot material was flushed from the reservoir during the previous run. The high values of R in run MSS-C-5 could have been caused by dissolution of this residual material in the condensate, even though early samples showed low values of R. This conclusion seems strengthened by results obtained for run MSS-C-6 in which the values of R were high initially and then decreased during the run.

Although these data are not conclusive, they indicate that polarization and entrainment effects are not important.

3.1.3 Difficulties Encountered

Surprisingly, only a few operational problems arose during the experimental program. Three significant difficulties that were encountered are discussed below.

During the second run, the salt feed line to the still became obstructed. After the run had been completed, the line was cut and a 5- to 10-g metallic deposit, consisting mainly of nickel and iron, was found at the point where the feed line enters the still. This line was replaced, and the still was operated for four additional runs. At the end of the operation, the feed line was again removed, and another metallic deposit

---

[5] M. E. Whatley *et al.*, *Unit Operations Section Quarterly Progress Report, January-March 1967*, ORNL-4139, p. 48.

was found at the same point. The composition and the appearance of the second deposit were similar to those of the first deposit; however, the feed line was not completely obstructed in this case. The cause for the deposition of metals in the feed line is not understood. One possible explanation, based on the observation that the higher fluorides of most elements are more volatile than their lower fluorides, is that the still pot is "reducing" with respect to the feed salt and thus leads to the deposition of metals at the inlet to the still pot.

During the fourth run, ZrF_4 vapor condensed in the vacuum line from the receiver and blocked it at the point where the 1-in. line joins the receiver. Subsequently, this line was cut, and the obstruction was removed. During the sixth run the vacuum line again became blocked, but the obstruction was removed by heating the line to 950°-1050°C without interrupting the run.

At the start of the fifth run, a malfunction of the tubular heater that was being used to melt the salt caused the dip line to melt while the distillation equipment was under vacuum. This type of failure will be avoided in future runs by electrically insulating the heating element from the line.

3.1.4 Postoperational Examination

Following the nonradioactive operation, metal thicknesses were measured around the still pot and at each end of the condenser (where high stresses were anticipated). These measurements were compared with those made prior to operation. The average of 225 measurements showed a decrease of 1.6 mils in wall thickness, with both positive and negative deviations from the original thickness. The largest differences were +9 mils and -8 mils. Distances between selected points on the equipment were measured both before and after operation of the still. The change in distance between two widely separated points was not found to be significant; the average change was 0.026 in. There was some indication that

the still pot had dropped to a slightly lower position. The rotation of lines between points at the opposite ends of the still was less than 1/2°. These results are acceptable. The measurements summarized above are recorded on drawings M-12173-CD-019D, M-12173-CD-020D, and M-12173-CD-021D.

Visual inspection revealed that the metal on the inside of the still pot was in good condition. The walls were shiny, and there was no evidence of pitting or cracking. Also, no evidence of physical change could be detected by means of radiography.

Corrosion specimens of Alloy 82, Hastelloy N, TZM, Haynes Alloy No. 25, and grade AXF-5QBG graphite were suspended in the vapor zone and in the liquid zone of the still pot during the six runs. At the conclusion of the nonradioactive experiments, these specimens were removed and delivered to the Metals and Ceramics Division for detailed examination. A preliminary report of this examination can be found in ref. 6.

3.1.5 Conclusions

The nonradioactive operation of the molten salt distillation equipment has led to the following conclusions:

1. Large molten-salt distillation equipment has been operated successfully for relatively short periods.
2. Measured distillation rates are adequate for the use of distillation as a process step. Measured vaporization rates were adequate for processing 15 ft^3 of salt per day in a still of reasonable size.
3. Concentration polarization and entrainment were not detected in these tests.
4. The reason(s) for the formation of metallic deposits in the salt feed line must be determined since such obstructions will disrupt long-term operation.
5. The condensation of volatile salt components and corrosion products in the cold vacuum lines would be a source of difficulty in long-term operation.

[6] MSR Program Semiann. Progr. Report Aug. 31, 1968, ORNL-4344, p. 282.

3.2 Frozen-Wall Corrosion Protection

B. A. Hannaford L. E. McNeese

A layer of frozen salt has been proposed[7] as a means for protecting the metallic walls of molten-salt processing equipment from a severely corrosive environment such as that which exists in a continuous fluorinator. In order to study this means of corrosion protection, we built and operated a 5-in.-diam column that contained electrical resistance heaters positioned along the center line of the column (to simulate a volume heat source resulting from the decay of fission products in the salt). A countercurrent flow of argon was used to produce the hydraulic effects of a gas (fluorine) rising through the molten salt. Heat removal was accomplished by forced-air cooling, or by a combination of radiation and natural convection.

The temperature distribution in the salt is a function of heat-generation rate and thermal conductivity and is shown in Fig. 3.5. The interface between molten salt and frozen salt is designated by R_1, and the inner and outer surfaces of the column are denoted as R_2 and R_3, respectively. For our experimental apparatus, heat generation within the frozen salt, A_2, was zero; the applicable expression for this case is designated as (2) in Fig. 3.5.

Typical experimental values for the temperature drop at R_1 were 2 to 5°C; the temperature drop across the frozen salt was 75 to 160°C. The temperature drop across the metal wall (less than 1°C) was disregarded.

In a series of experiments we demonstrated that a frozen salt layer can be formed and maintained with conditions of fluid flow and heat transfer approximating those expected for processing fuel from a 1000-Mw (electrical) MSBR.

---

[7] R. W. Kessie *et al.*, *Process Vessel Design for Frozen-Wall Containment of Fused Salt*, ANL-6377 (1961).

ORNL DWG 68-3350 R1

(1) $T = T_L + \frac{R_1^2}{2k_2}(A_1 - A_2)\ln\frac{R_1}{r} + \frac{A_2}{4k_2}(R_1^2 - r^2)$

FOR $A_2 = 0$, AND $A_1 = \frac{Q}{\pi R_1^2}$,

REDUCES TO

(2) $T = T_L + \frac{Q}{2\pi k_2}\ln R_1 - \frac{Q}{2\pi k_2}\ln r$

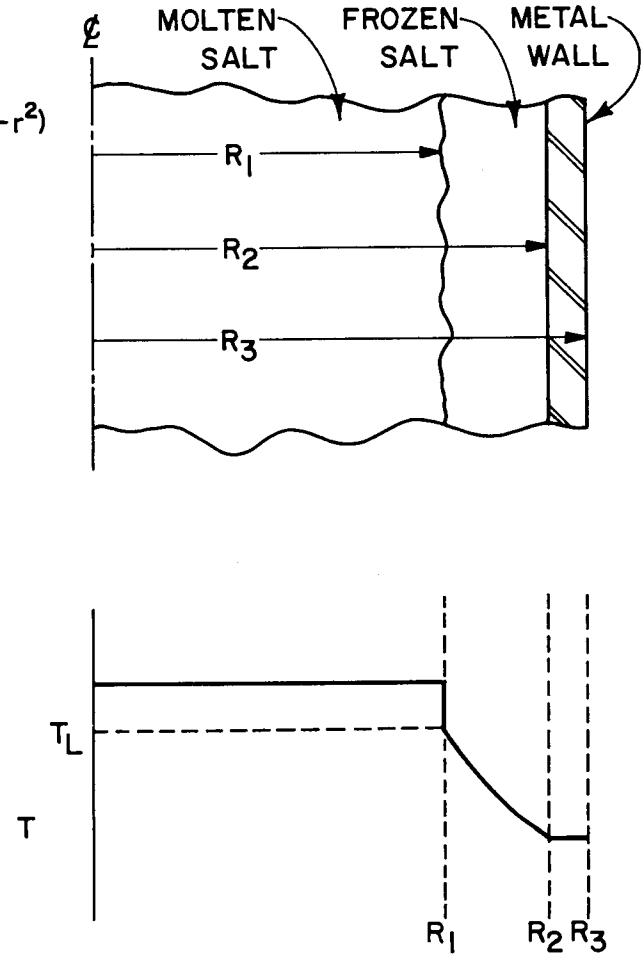

Fig. 3.5. Steady-State Frozen Salt Temperature for Radial Heat Flow. T_L = liquidus temperature; A_1 = volumetric heat generation rate in the molten salt phase; A_2 = volume heat generation rate in the frozen salt phase; Q = heat removal rate per unit length of the column; r = radius variable; k_2 = thermal conductivity of frozen salt.

3.2.1 Experimental Equipment and Procedures

The test vessel was a column having a diameter (5 in.) and a height (8 ft) approximately equal to those of a plant-scale fluorinator. Since the principal objective of the work was to demonstrate that a reasonably uniform layer of frozen salt could be established and maintained at expected heat-generation rates, an inert gas was substituted for fluorine; this greatly simplified the experiment. The column had two 21-in.-long test sections (Fig. 3.6); each contained four internal thermocouples, located 1/4, 1/2, 3/4, and 1-1/2 in. from the inside wall, to indicate the location of the melt-solid interface. The principal heat source, which simulated a volume heat-generation source within the salt, consisted of a 3/4-in. Inconel pipe that contained three Calrod heaters and was capable of a maximum output of about 6400 w. All external surfaces of the column were wrapped with Calrods and covered with insulation in order to control the temperature of the outside wall. In most experiments, only the set of external heaters located nearest the bottom of the column was needed to supplement the internal heater. The surface was cooled by air forced through spirally wound coils of 3/8-in.-diam nickel tubing tacked to the pipe surface.

The experimental procedure consisted of metering molten salt, a 66-34 mole % $LiF-ZrF_4$ mixture that has a liquidus temperature of about 595°C, to the top of the column by controlled argon pressurization of the feed tank. The desired liquid level in the column was maintained by a jackleg, which discharged to the salt receiver. A countercurrent flow of argon was introduced to the column through an inlet located about 1 ft above the bottom of the column. Heat input and air cooling rates were adjusted until steady-state temperatures were established in the test sections. Steady state was defined as a period of 30 to 90 min during which individual internal temperatures and important surface temperatures varied within 2°C. Values for the heat flux in the test sections were calculated from the temperature rise in the metered cooling air. Prior to the concluding experiments, the thermal insulation was removed from the test section so that heat was transferred by radiation and natural convection. For these

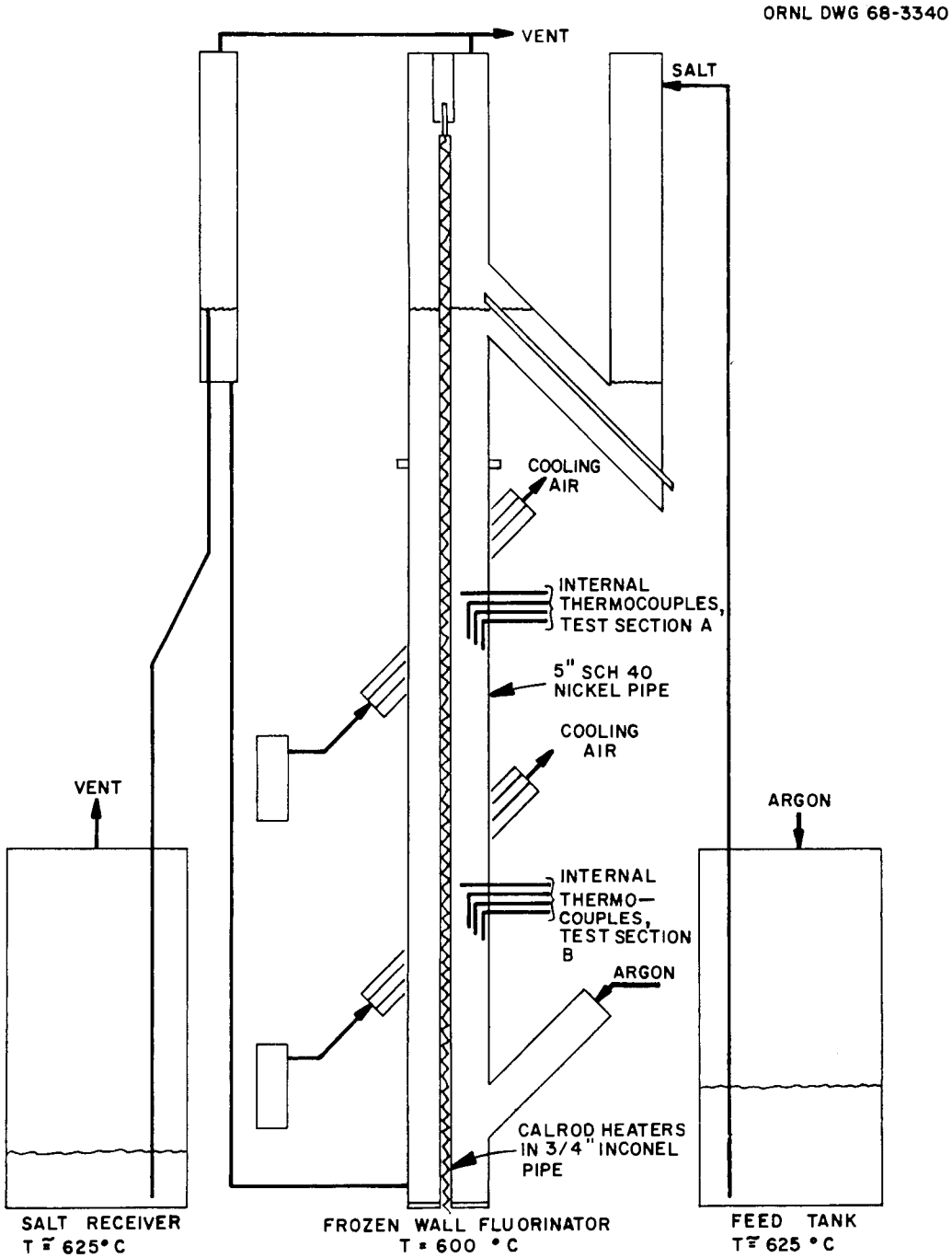

Fig. 3.6. Experimental Equipment for Studying Formation of Frozen Salt Layer for Corrosion Protection. Height of column = 8 ft. Height of each test section = 1.75 ft.

experiments, the heat flux was inferred from the difference between the total heat input and the previously measured heat losses from the insulated portions of the column.

3.2.2 Experimental Results

The principal results are summarized in Table 3.3. The apparent thermal conductivity of the frozen-salt layer was calculated for each experiment, thus providing a check of the consistency of the data. Calculated thermal conductivities for experiments 3 and 11 in the first group of experiments (all run at a relatively low argon flow rate) deviated somewhat from the values obtained in the other experiments. This implies an error in the estimated salt thickness or in the calculated heat flux.

In the third group of experiments (21 through 29), the conductivities were markedly higher, perhaps reflecting the uncertainty in the heat flux. (For this group of experiments, heat flux was considered to be the difference between the heat input and the estimated total of all other heat losses.) Assuming a value for k_2 of about 2.7 to be representative, the calculated salt thickness for experiment 22 would be 0.11 in. This is consistent with the estimate of less than 0.44 in. based on the position of the shallowest internal thermocouple. The calculated salt thicknesses varied from 0.11 to 1.10 in.; most of the values were in the range 0.77 to 1.10 in.

In experiments 23 and 27 the salt was rapidly drained from the column at the conclusion of the steady-state period; after cooling, the column was examined by radiography. An x-ray photograph showed that, over the 3-1/2-in. elevation covered by the array of internal thermocouples, the salt thickness tapered from 0.80 in. to 0.65 in. (see Fig. 3.7). The thickness of the salt layer in the plane of the 1/2-in.-deep thermocouple was measured (from the x-ray) and found to be in good agreement with the value obtained by the usual method for determining thickness (i.e., temperature measurements). The latter method is illustrated in Fig. 3.8.

Table 3.3. Heat Transfer from Test Section A Operated with a Frozen Wall

Conditions: salt flow rate, 0-8 liters/hr
bulk salt mixture, $LiF-ZrF_4$ (66-34 mole %)
liquidus temperature (T_L), 595°C
inside radius of column, R_2, 2.52 in.

Experiment	Heat Flux, Q (w/ft)	Equivalent Heat Generation Rate, A_1 (Btu hr^{-1} ft^{-3})	Temperature Drop, ($T_L - T_{R_2}$) (°C)	Frozen Salt Thickness,[a] ($R_2 - R_1$) (in.)	Thermal Conductivity,[b] k_2 (Btu hr^{-1} ft^{-1} °F^{-1})	Approximate Length of Test Section A (in.)
		A. Cooling by Air Flowing Through Coils. Argon Flow Rate, 30 liters/hr				
1	925	60,000	123	0.94	1.06	21
2	995	78,000	148	1.10	1.17	21
3	860	47,000	127	0.83	0.81	21
4	1130	81,000	156	1.04	1.16	21
5	1040	73,000	146	1.02	1.12	21
7	770	46,000	93	0.91	1.12	21
8	660	45,000	88	1.00	1.14	21
9	1170	60,000	114	0.77	1.13	21
11	810	44,000	109	0.83	0.89	21
		B. Cooling by Air Flowing Through Coils. Argon Flow Rate, 120 liters/hr				
12	1025	62,000	140	0.92	1.00	21
13	815	40,000	77	0.73	1.10	21
16	1220	57,000	112	0.69	1.05	21
17	1635	89,000	166	0.82	1.17	21
18	610	41,000	103	0.99	0.89	21
19	516	34,000	85	0.99	0.91	21
20	1545	82,000	140	0.81	1.29	21
		C. Cooling by Radiation plus Natural Convection. Argon Flow Rate, 120 liters/hr				
21	2620	140,000	89	0.79	3.33	14
22	3600	110,000	18	< 0.44[c]	11.6	14
23	2500	130,000	136	0.80 $\boxed{0.74}$[d]	2.12	14
24	2580	160,000	136	0.91	2.57	18
26	2970	160,000	115	0.80	2.99	18
27	2970	190,000	127	0.94 $\boxed{0.95}$[d]	3.28	18
28	2270	150,000	160	0.99	2.12	21
29	2900	140,000	107	0.69 $\boxed{0.44}$[e]	2.61	21

[a]Determined by extrapolating from T_{R_2} (assumed equal to the surface temperature) through the temperature of nominal 1/2-in. thermocouple (position by direct measurement was 1.86 in. from center line) to liquidus temperature of 595°C.

[b] $$k_2 = \frac{Q \ln (R_2/R_1)}{2\pi(T_L - T_{R_2}}.$$

[c]All internal thermocouples were above 595°C; therefore, (R_2-R_1) is less than the actual position of the shallowest thermocouple.

[d]Salt thickness at the elevation of the nominal 1/2-in. thermocouple, as measured from x-ray of test section.

[e]Salt thickness at the elevation of the nominal 1/2-in. thermocouple, as measured directly from cross-sectioned column.

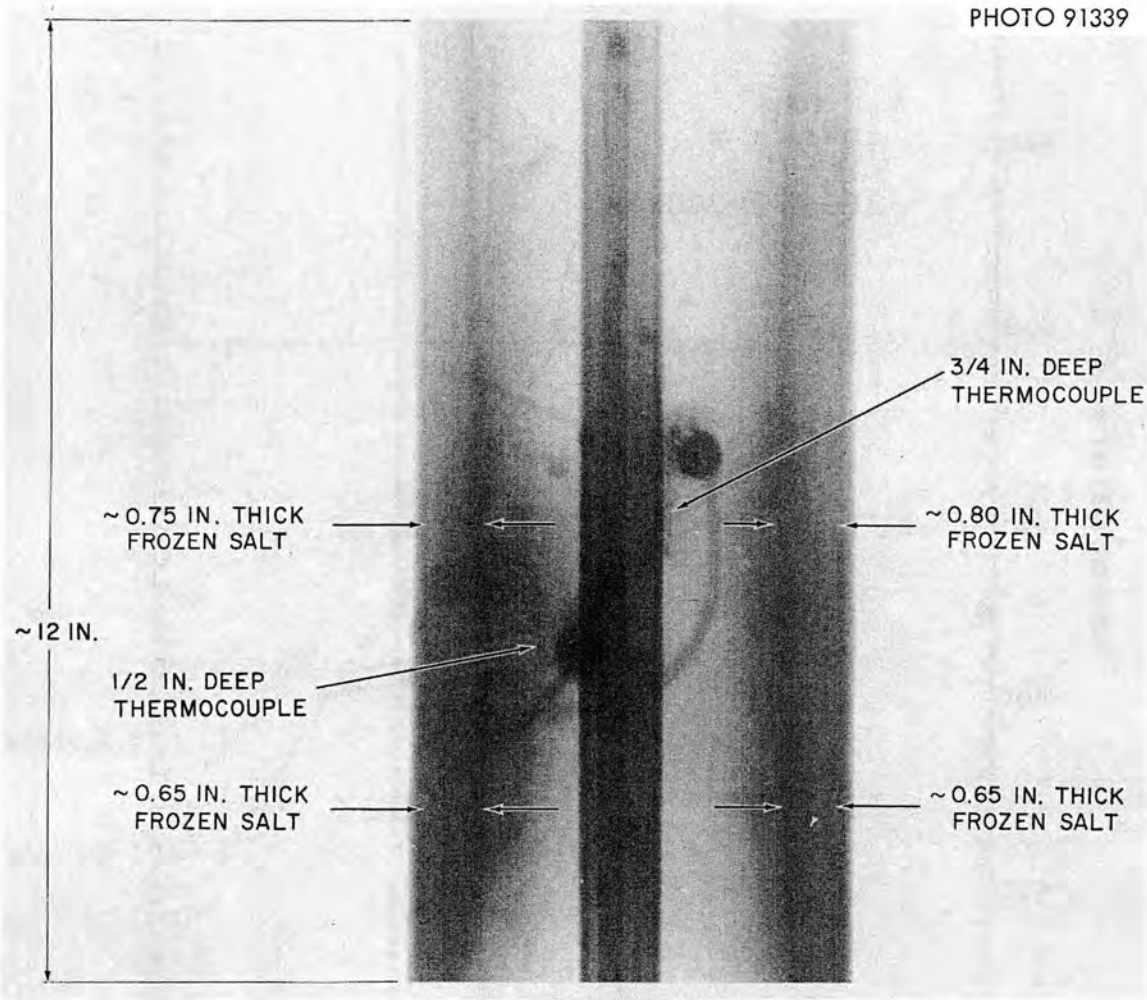

Fig. 3.7. X-Ray Photograph of 5-in.-diam Column Made Following Experiment 23, After Removal of the Molten Salt and Cooling. Thickness of the frozen salt layer decreases toward the insulated ends of the test section. Length of uninsulated test section, ~ 14 in.

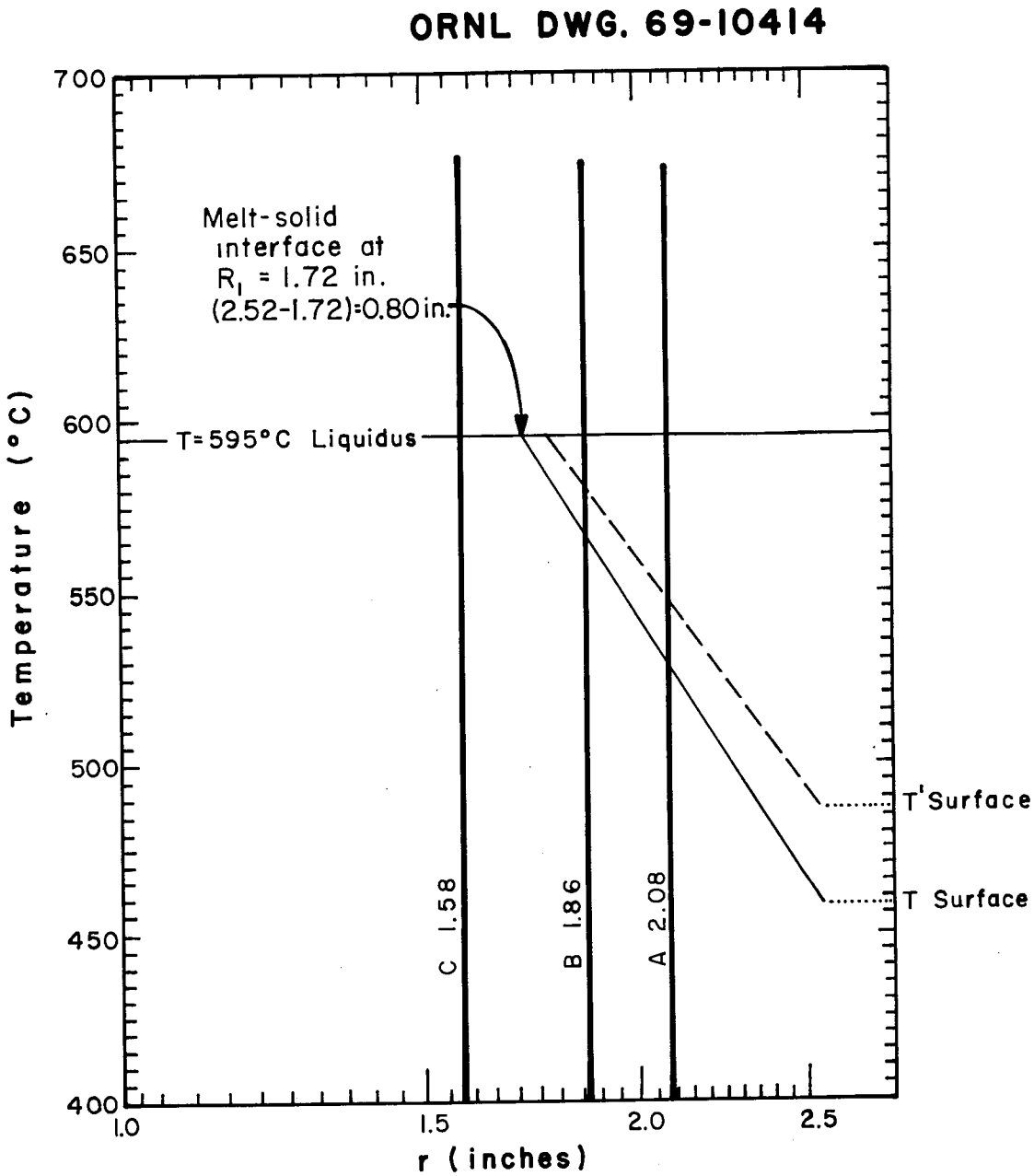

Fig. 3.8. Salt Temperature vs Radius in 5.04-in.-ID Column. Thickness of frozen salt = 0.80 in. by the preferred method of extrapolating from a surface temperature, through the temperature of adjacent thermocouple B, to the liquidus temperature (experiment 25).

Extrapolation of the temperature through thermocouple B was preferred because there was some evidence that the position of thermocouple A had shifted during the course of the experiments. The more obvious method of locating R_1, the solid-liquid interface, by using all three internal thermocouples (i.e., the method originally intended) was not feasible for two reasons: (1) The surface of the column was not at a uniform temperature, and the internal thermocouples were not located in a single horizontal plane. (2) An internal thermocouple located as much as ~ 0.2 in. deeper than the nominal interface would affect the temperature distribution in its vicinity and would collect a layer of frozen salt because of heat transfer along the thermocouple.

The final experiment (experiment 29) provided an illustration of (2) above. The usual method for determining frozen salt thickness indicated a value of 0.69 in. (Table 3.3). Examination of the test section at the conclusion of this experiment showed that a perturbation of the otherwise uniform 0.44-in.-thick salt layer existed at the locations of internal thermocouples A and B. The upper test section was sawed into sections to permit examination of the frozen salt layer, the internal thermocouple location, etc. (Fig. 3.9). The salt thickness was found to be very uniform over this central portion of the test section; however, two separate frozen salt layers were observed (see Fig. 3.10). The inner, dark layer was apparently deposited during the 1-hr period required to drain the molten salt from the column (after removing the heat input). The low drain rate was caused by obstructions in the drain line; these obstructions limited the salt flow rate during the later runs to 3 liters/hr or less. The outer layer of frozen salt was present under steady-state conditions. Its thickness was essentially uniform, varying from 0.40 to 0.45 in., around the entire circumference. A similar uniformity in thickness along a 6-in. part of the test section is shown in Fig. 3.11. The dislocation of the original molten-salt--frozen-salt interface in the vicinity of the thermocouple well can also be seen; it amounts to a radial displacement of about 1/8 in. from the unperturbed interface.

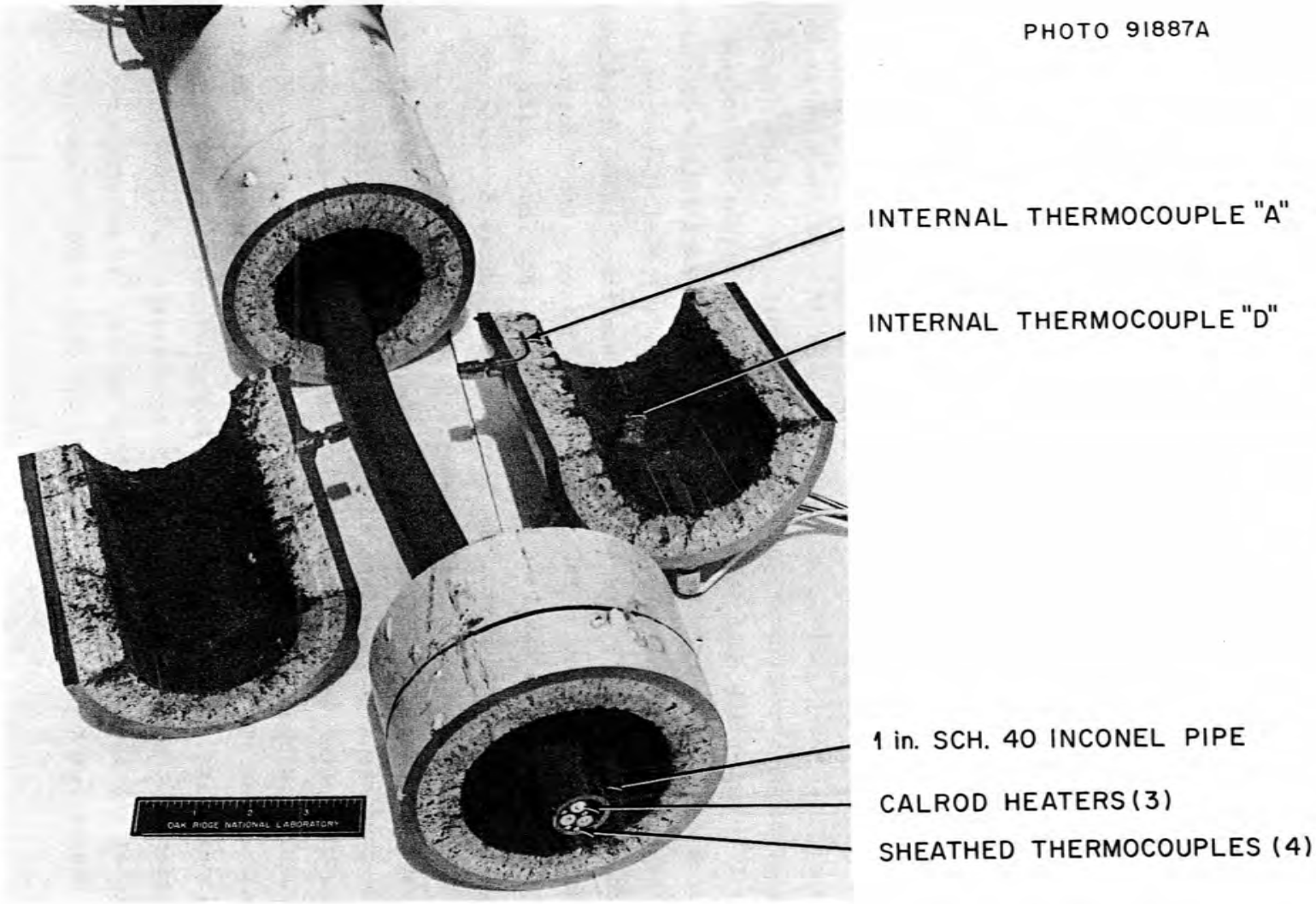

Fig. 3.9. View of the Central Portion of the Test Section. Upper end of the test section is in the foreground.

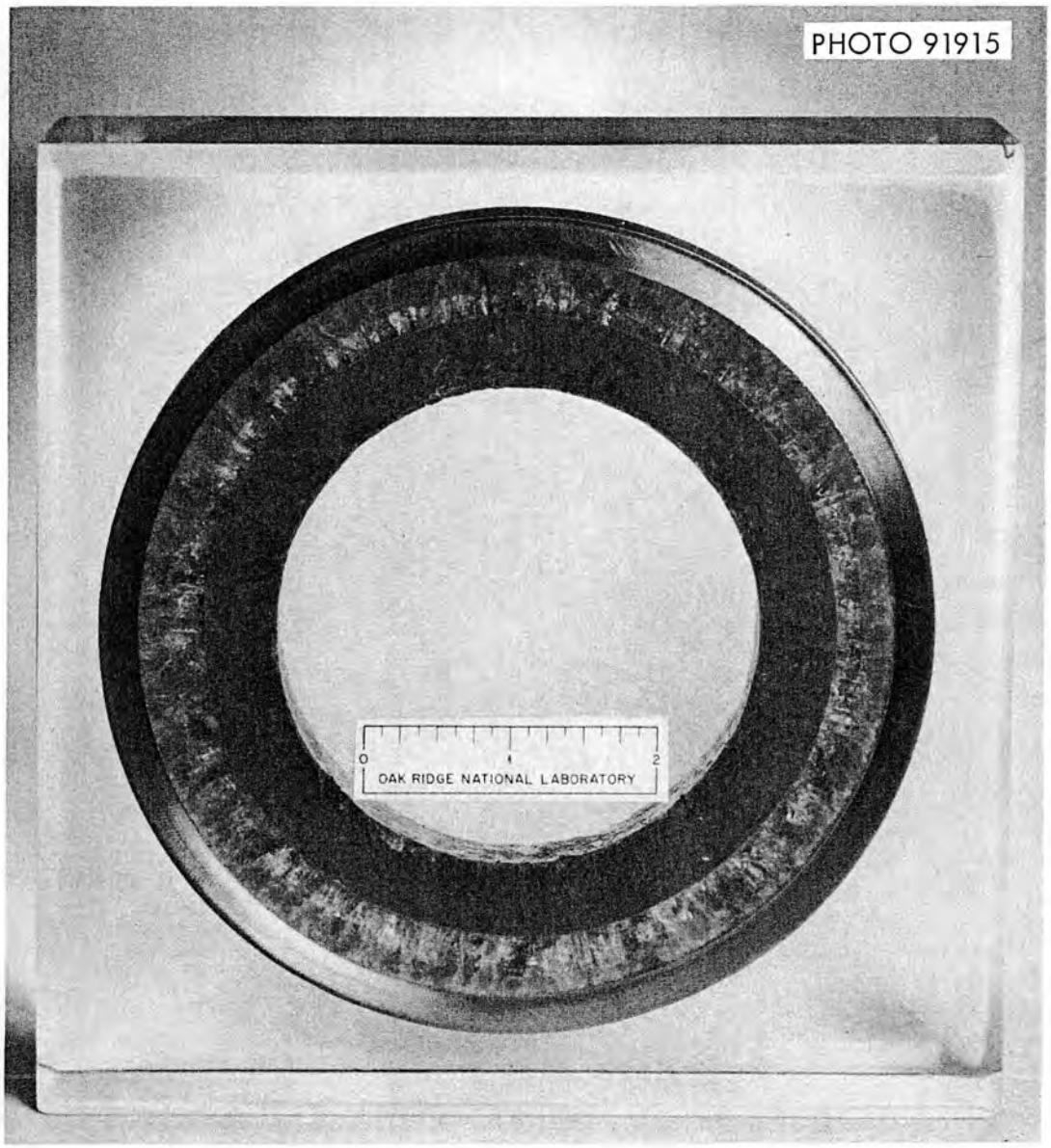

Fig. 3.10. Cross Section of Column Showing the Frozen Salt Layers. This portion was cast in plastic after being removed from a plane about 2 in. below thermocouple A.

PHOTO 91885A

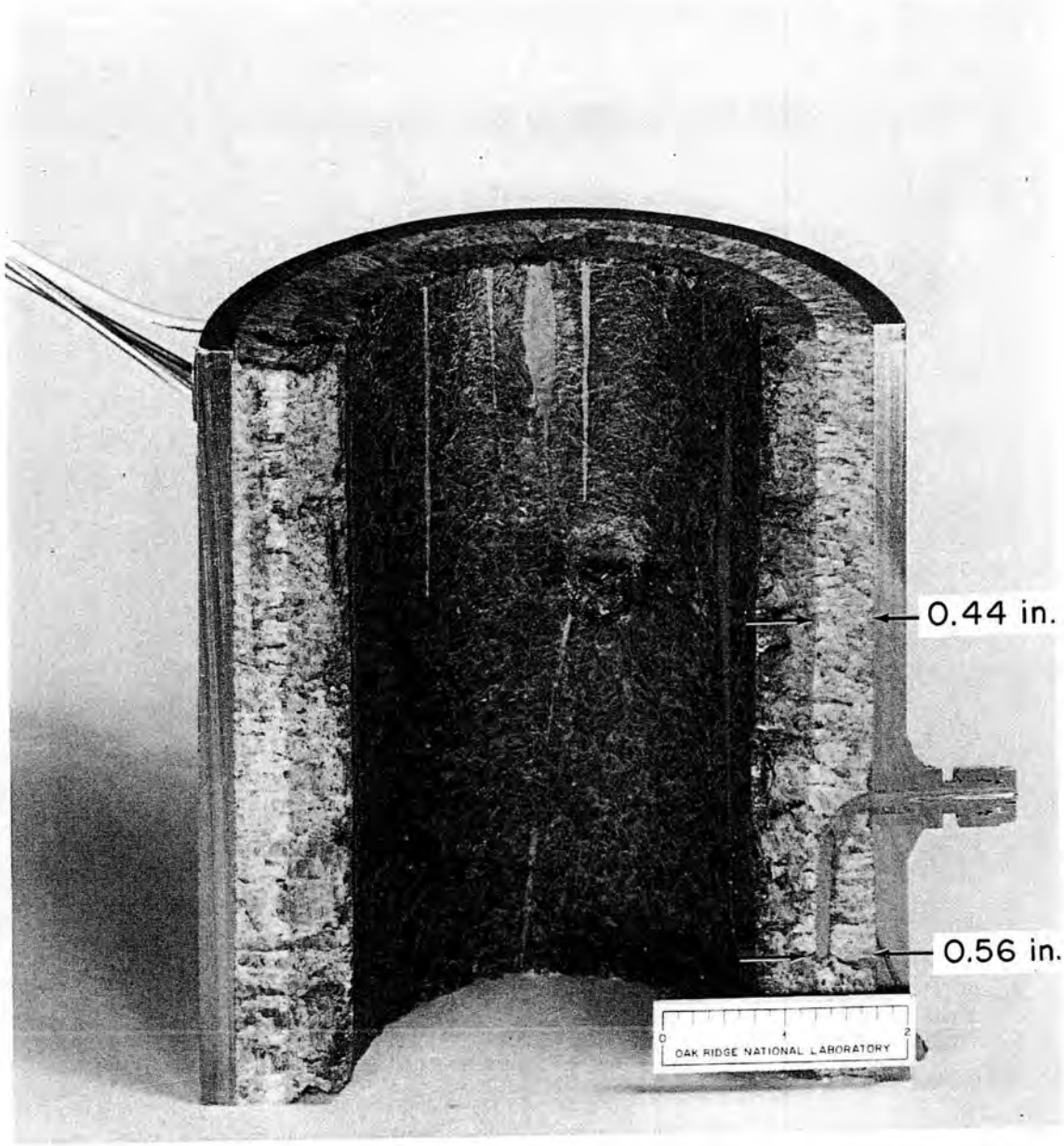

Fig. 3.11. Central 6-in.-long Portion of Test Section A Following Experiment 29. Presence of internal thermocouple A caused a local increase in the thickness of an otherwise uniform salt layer.

Measurements of the concentricity of the frozen layer throughout approximately a 30-in. length of the upper test section indicated that the off-axis feed point for the argon caused no undesirable effects on the uniformity of the thickness of the frozen layer.

It may be noted (Table 3.3) that most experiments were run at estimated volume heat generation rates that were greater than the reference value of 50,000 Btu hr^{-1} ft^{-3}. This reflects the fact that, at lower values, there was a tendency for frozen salt to block the column in such a manner that argon being fed to the bottom of the column exited through the salt outlet line. This was particularly evident when the lower test section, adjacent to the argon inlet, was being cooled; for this reason, data from the lower test section are not included in Table 3.3.

We also demonstrated operation with a layer of frozen salt on the wall of the argon inlet that represented a fluorine feed point. When desired, the set of six surface temperatures on the nozzle could be maintained below the liquidus temperature of the salt during the period that argon was fed to the column. This implies that the molten salt in contact with the wall would have formed a protective layer of frozen salt; however, no internal thermocouples were located in this section.

In summary, it can be stated that the general objectives for this series of experiments were achieved. It was shown that molten salt and a gas can be contacted countercurrently in equipment suitable for continuous fluorination. Also, it was shown that, under expected operating conditions, a layer of frozen salt can be easily and predictably deposited and maintained on surfaces contacted by the salt. The frozen salt layer was found to be adherent and stable, and it should provide sufficient corrosion protection to allow operation over extended periods.

3.3 Studies of a Simulated Molten-Salt--Liquid-Bismuth Contactor

J. S. Watson L. E. McNeese

The proposed method for removing protactinium and fission products from the fuel of single-fluid MSBR's or from the blanket salt of two-fluid reactors involves reductive extraction using liquid bismuth containing lithium and thorium reductants. Equipment is needed to efficiently contact countercurrent streams of fuel salt and bismuth. The properties of these latter fluids are considerably different from those of aqueous and organic fluids conventionally used in liquid-liquid extraction equipment. For example, the difference in densities of the salt and metal phases will be 5.5 to 7.5 g/ml, whereas aqueous-organic systems have density differences of 0.05 to 0.2 g/ml between the phases. Similarly, the interfacial tension between bismuth and molten salt could be a factor of 10 greater than that of aqueous-organic systems.

Since the correlations used to design liquid-liquid extraction systems are based upon conditions far removed from those of current interest, experimental data from systems similar to the molten-salt--bismuth system are needed. Because experiments with bismuth and molten salt are difficult and expensive, a mercury-water system is being used to allow selection of contactor designs for testing actual process fluids. This simulated system will provide quantitative data on flooding rates, pressure drop, holdup, and backmixing, as well as qualitative information on flow patterns and drop size.

One similar study has been reported; Johnson and co-workers[8] at Argonne National Laboratory studied a column that was packed with 3/16-in. Berl saddles, using water and Wood's metal. Their observed flooding rates were not adequately predicted by conventional correlations.

---

[8] T. R. Johnson, F. G. Teate, D. R. Gorth, and P. J. Mack, Chemical Engineering Division Semiannual Report, July-December 1966, ANL-7325, pp. 30-32.

The experimental equipment assembled for our study is shown schematically in Fig. 3.12. Mercury is pumped from a hold tank into the column by a diaphragm pump* containing tantalum check valves. The pump body and all the piping are fabricated of stainless steel. At present, either tap water or distilled water can be used. Preliminary tests showed the results to be more consistent when distilled water is used. The water is not recirculated.

The column consists of a 2-ft length of 1-in.-diam glass pipe. The end sections are expanded to 2 in. diameter in order to produce lower velocities (for coalescence) and to provide space for the inlet and outlet lines. The first material evaluated for use in column packing consisted of Teflon Raschig rings (3/16 in. OD and 3/16 in. long, with 1/8-in. holes). Teflon and polyethylene will probably be chosen for most of the packing materials to be studied because these materials are not wet by bismuth or molten salt. Neither of the phases is expected to wet the materials chosen for the process contactor, which will probably be constructed of graphite or molybdenum.

The mercury interface at the bottom of the column is set approximately by a jackleg on the mercury outlet. The exact position of the interface is then used to measure the pressure drop through the column.

The water flow rate is measured by rotameters on the inlet line, and the mercury flow rate is determined by setting the pump stroke length. This method of setting the mercury rate is one of the inconvenient features of the system. The pump has only four settings, and although settings halfway between these marks can be estimated, the mercury rate cannot be continuously varied.

Flooding is detected by observing the pressure drop across the column and/or by noting behavior of the rotameter. Below the flooding point, the water rotameter can be set at a desired flow rate, where steady readings of pressure drop and flow rate are observed. However, when flooding is

*Hills-McCanna Masterline Model 21; manufactured by the Hills-McCanna Co., Carpentersville, Ill.

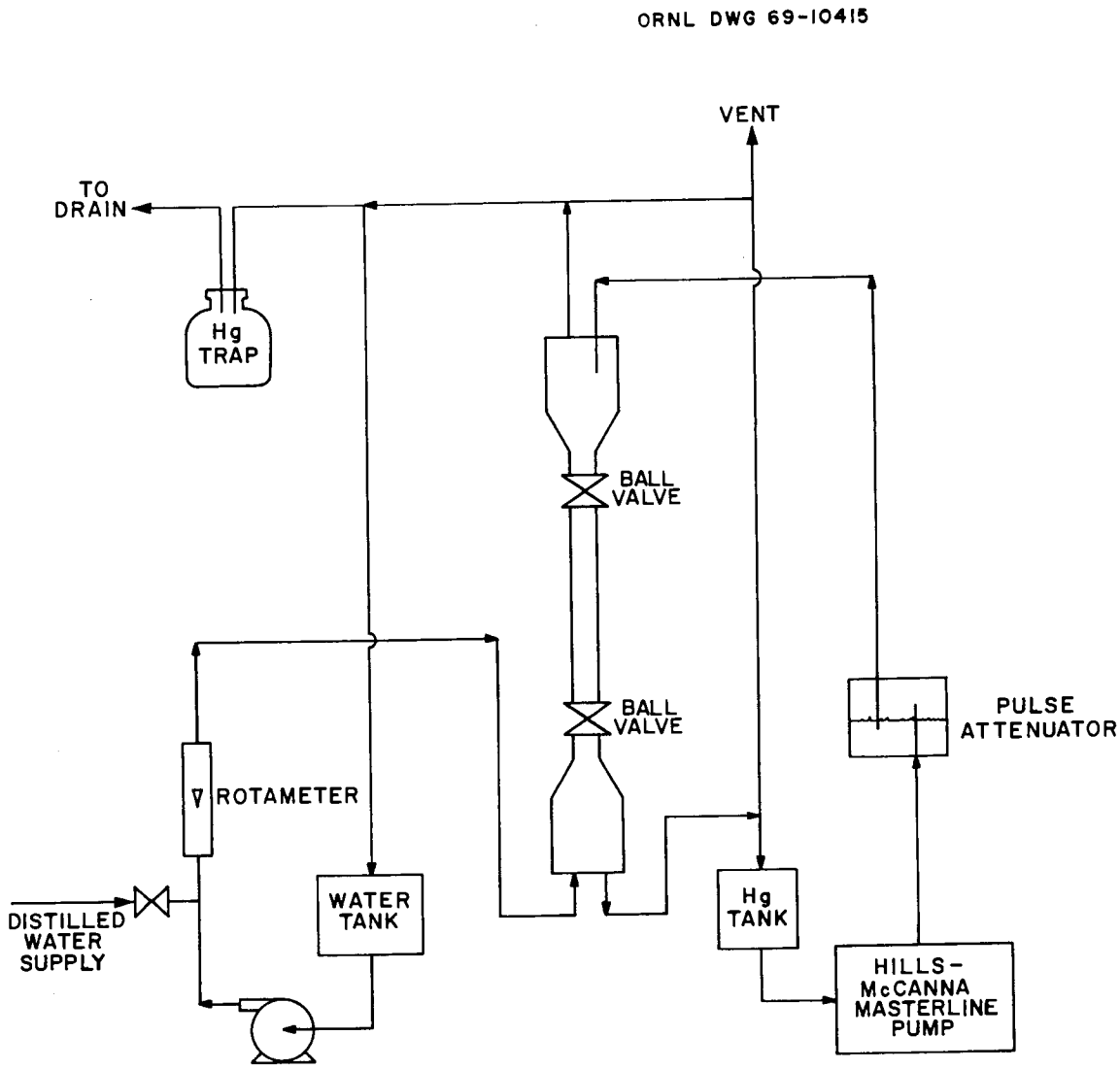

Fig. 3.12. Schematic of the Simulated Molten-Salt--Bismuth Extractor.

reached, the pressure drop increases with time because the holdup of mercury in the column is increasing. With the water supply currently in use, this causes the water flow rate to decrease below the flooding rate. After the water flow rate has decreased, the accumulated mercury drains from the column and the water flow rate returns to approximately the original setting. Then mercury begins to accumulate again, and the cycle is repeated. The alternate accumulation of mercury in, and draining of mercury from, the column can also be observed in a qualitative manner by simply watching the column. In this study, flooding is defined as the point at which cyclic accumulation can be detected via the pressure drop or rotameter readings. This definition may be somewhat arbitrary because, at lower flow rates, accumulation and draining can be observed at local points within the column; however, these local situations do not result in significant variations in pressure drop.

The initial experiments in this study were made with 3/16-in.-OD and 1/8-in.-ID Raschig rings that were approximately 3/16 in. long. In these experiments, the mercury did not flow down the column in discrete drops but was constantly coalescing and redispersing. Figure 3.13 shows a view of the column in operation. This type of dispersed-phase behavior is typical for small packing material.[9] When larger packing is used, the dispersed phase forms small drops that remain intact as they traverse the column. Small drops are usually preferred because they result in a higher interfacial area; however, if the mass-transfer resistance in the dispersed phase is high, the other operating mode may be preferred because coalescence and redispersion cause mixing of the dispersed phase.

The flooding data obtained with 3/16-in. rings are shown in Fig. 3.14 as horizontal bars that bracket the flooding rate. In obtaining these data, the metal flow rate was held constant, and the water flow rate was increased in increments until flooding was detected. The left side of the bar represents the last measurement made before flooding occurred, and

---

[9] F. R. Dell and H. R. C. Pratt, "Part I. Flooding Rates for Packed Columns," Trans. Inst. Chem. Engrs. (London) 29, 89-109 (1951).

PHOTO 92762

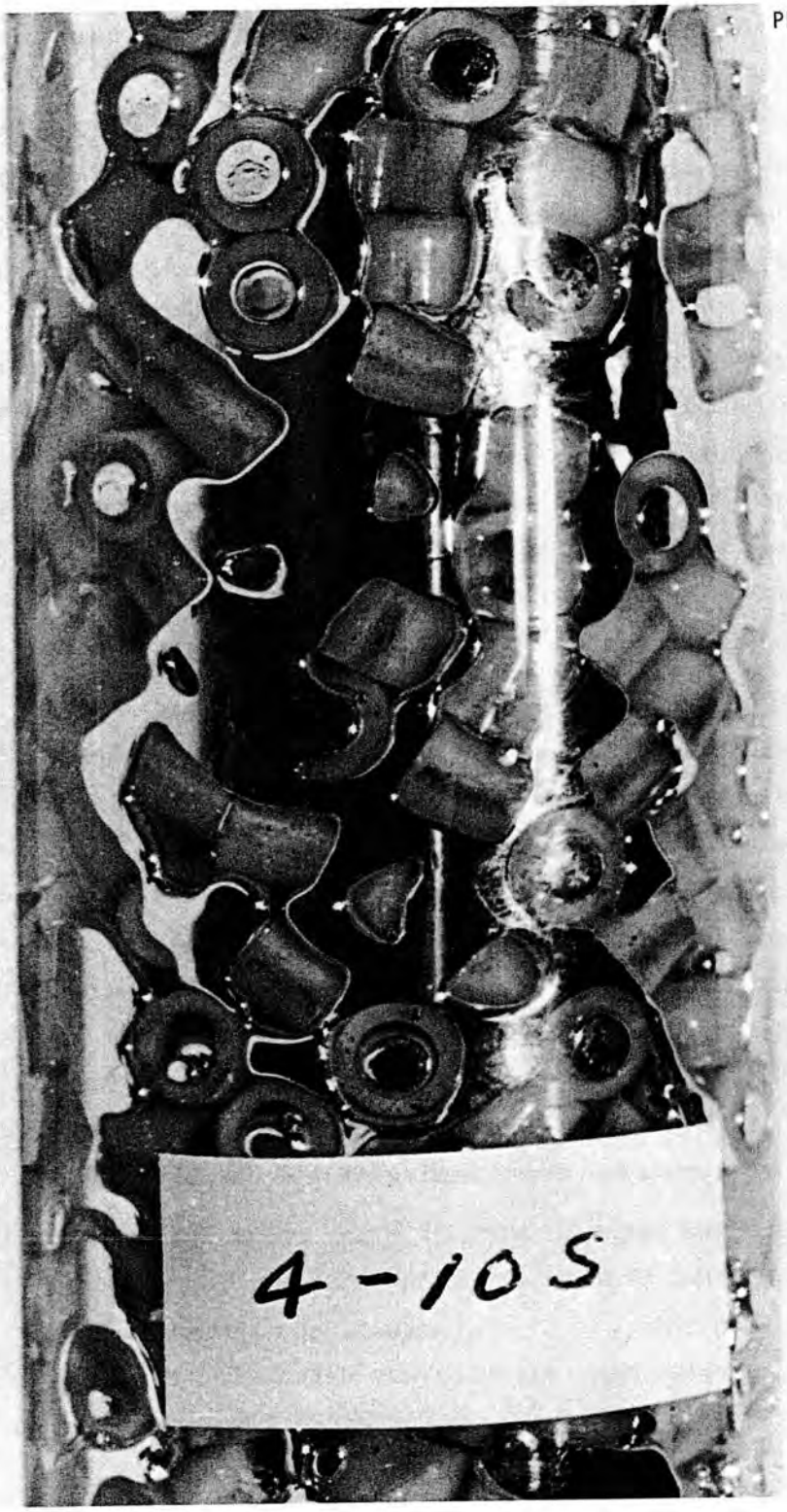

Fig. 3.13. Mercury-Water Column Operated with 3/16-in. Polyethylene Raschig Rings.

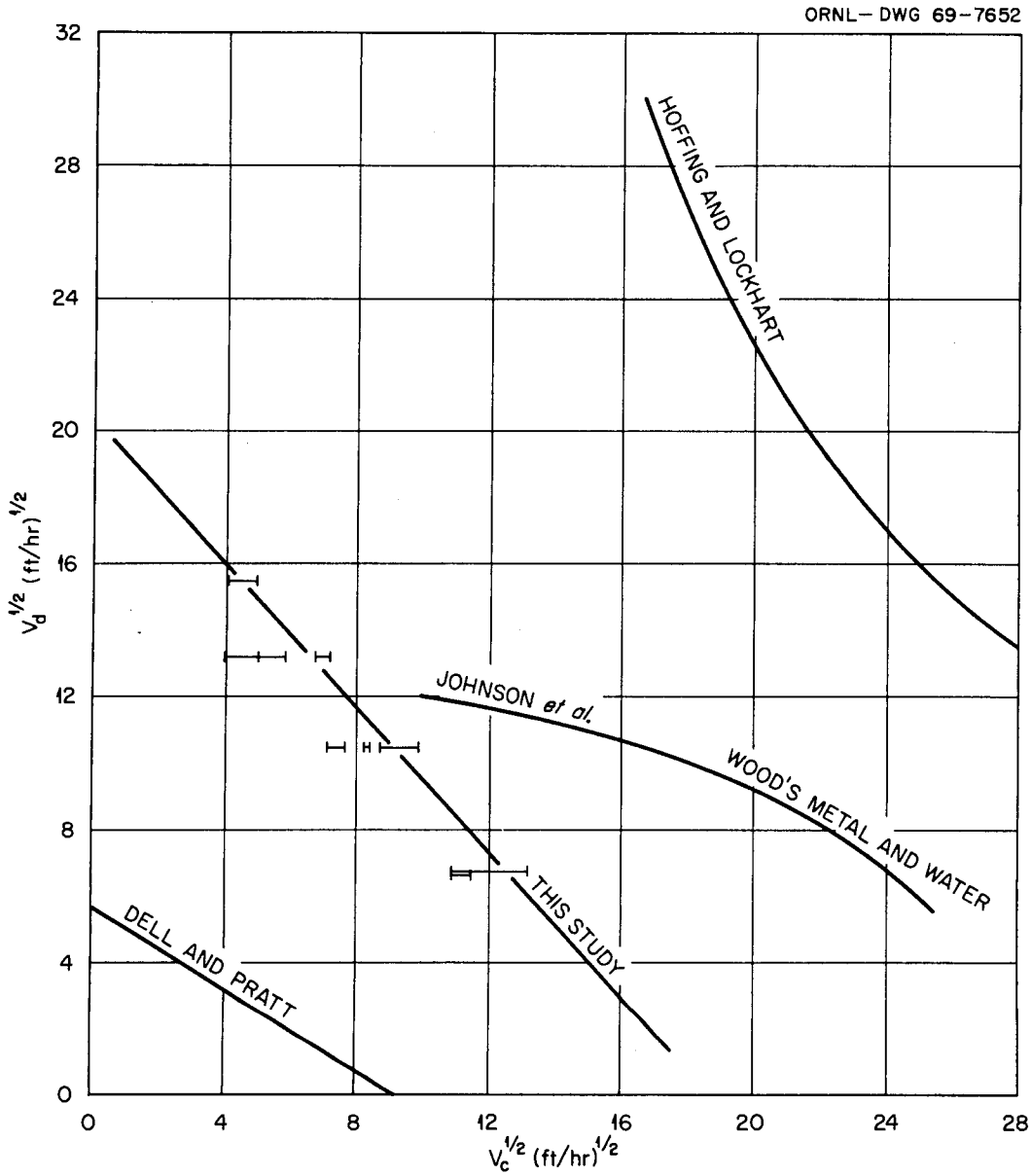

Fig. 3.14. Flooding Data Obtained by Using 3/16-in. Raschig Rings in the Column.

the right side represents the condition at which flooding was first detected. The square roots of the flow rates, rather than the flow rates themselves, were plotted since previous investigators[9] have shown that such a plot generally yields a straight line. Although there is scatter in our results, the values are fitted reasonably well by a straight line, using this method. Two frequently used correlations are shown for comparison: that of Dell and Pratt[9], and that of Hoffing and Lockhart.[10] It is obvious that neither of these correlations falls close to our data; furthermore, the two correlations do not agree with each other. This illustrates the inaccuracy that is inherent in extrapolating conventional correlations to high densities and interfacial tensions. For comparison, Fig. 3.14 also shows a curve that approximates the experimental data obtained by Johnson and co-workers[8] (at Argonne National Laboratory), who used 3/16-in. Berl saddles with Wood's metal and water. Their data most closely approach the conditions of current interest. The pressure-drop measurements with 3/16-in. rings are plotted in Fig. 3.15. Pressure drop, which is related to dispersed-phase holdup and flooding, can be easily measured in the salt-bismuth system as well as in the simulated system.

3.4 Electrolytic-Cell Development

M. S. Lin L. E. McNeese

The use of an electrolytic oxidation-reduction cell has been proposed for reducing thorium and lithium into bismuth, and for oxidizing materials from bismuth streams.[11, 12] At the anode side of the cell, materials such as uranium would be oxidized to uranium fluoride in the presence of a salt stream and would then be returned to the reactor. At the cathode

---

[10] E. H. Hoffing and J. Lockhart, "A Correlation of Flooding Velocities in Packed Columns," Chem. Engr. Progr. 50, 95-103 (1954).

[11] MSR Program Semiann. Progr. Rept. February 29, 1968, ORNL-4254, p. 248.

[12] Chem. Technol. Div. Ann. Progr. Rept. May 31, 1968, ORNL-4272, p. 17.

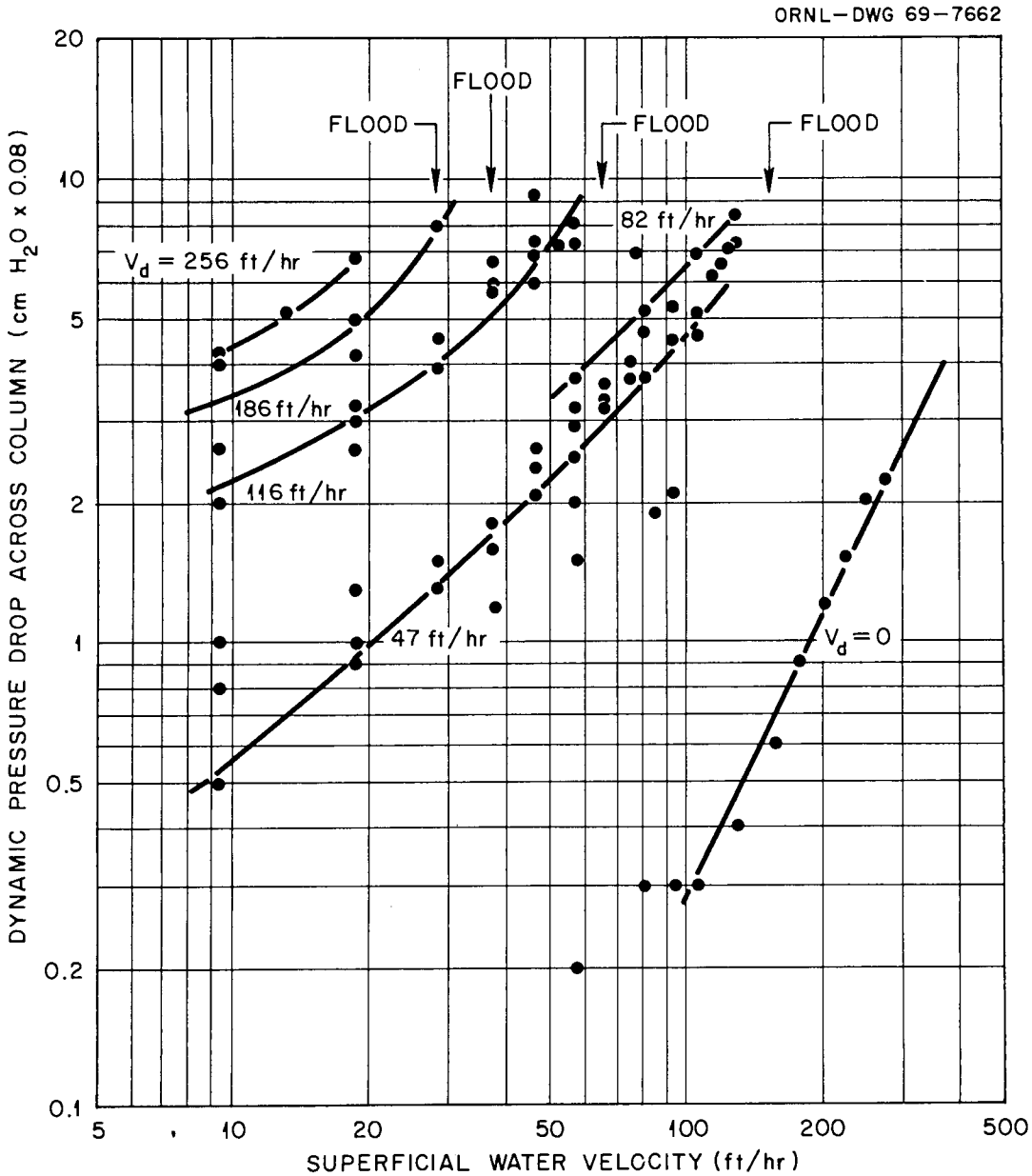

Fig. 3.15. Dynamic Pressure Drop Across Column Packed with 3/16-in. Raschig Rings.

side of the cell, LiF or ThF_4 would be reduced into the bismuth stream for use in the reductive extraction column.

One problem associated with cell operation is finding a suitable anode material. Since bismuth is the carrier of extracted materials at the column exit, and of reductant at the column inlet, it is logical to use bismuth as the cathode and bismuth containing extracted materials as the anode. Since the concentration of extracted materials in the bismuth is approximately 0.003 mole fraction, the estimated maximum current density is 0.27 amp/cm^2 (assuming a uranium diffusivity of about 2.5×10^{-5} cm^2/sec in bismuth,[13] a diffusion layer thickness of 5×10^{-3} cm, and an atomic volume of 21.3 cc/g-atom for bismuth). This current density is lower than desired.

A better approach is to oxidize bismuth to bismuth fluoride at the anode. In this case, the salt stream leaving the cell will contain bismuth fluoride, which will then be contacted with the bismuth stream containing extracted materials. This will convert the extracted materials to fluorides and the bismuth fluoride to bismuth. Such an arrangement will eliminate the limitation on current caused by the rate of transfer of the minor component to the anode surface.

In addition to a compatible anode, the electrolytic cell requires electrical insulation of the anode from the cathode. If bismuth flows from the anode to the cathode, a device to break the flow will also be essential.

An electrolytic cell has been designed (Fig. 3.16) and fabricated. In general, mild steel was used as the material of construction. The bismuth cathode is contained by a mild-steel plate (with overflow weirs) that is welded to the interior of the cell. The bismuth "flow-splitter" and the anode are fabricated from one piece of quartz and are located above the cathode. Bismuth entering the cell (Fig. 3.16) flows into the splitter compartment. A small portion of the bismuth flows into the anode below the splitter, while the remainder overflows into the cathode. The cell body is at the potential of the cathode, which is grounded. The anode is connected to a power supply through a molybdenum rod covered by a quartz

[13] J. C. Hesson, H. E. Hootman, and L. Burris, Jr., Electrochem. Technol. 3, 240 (1965).

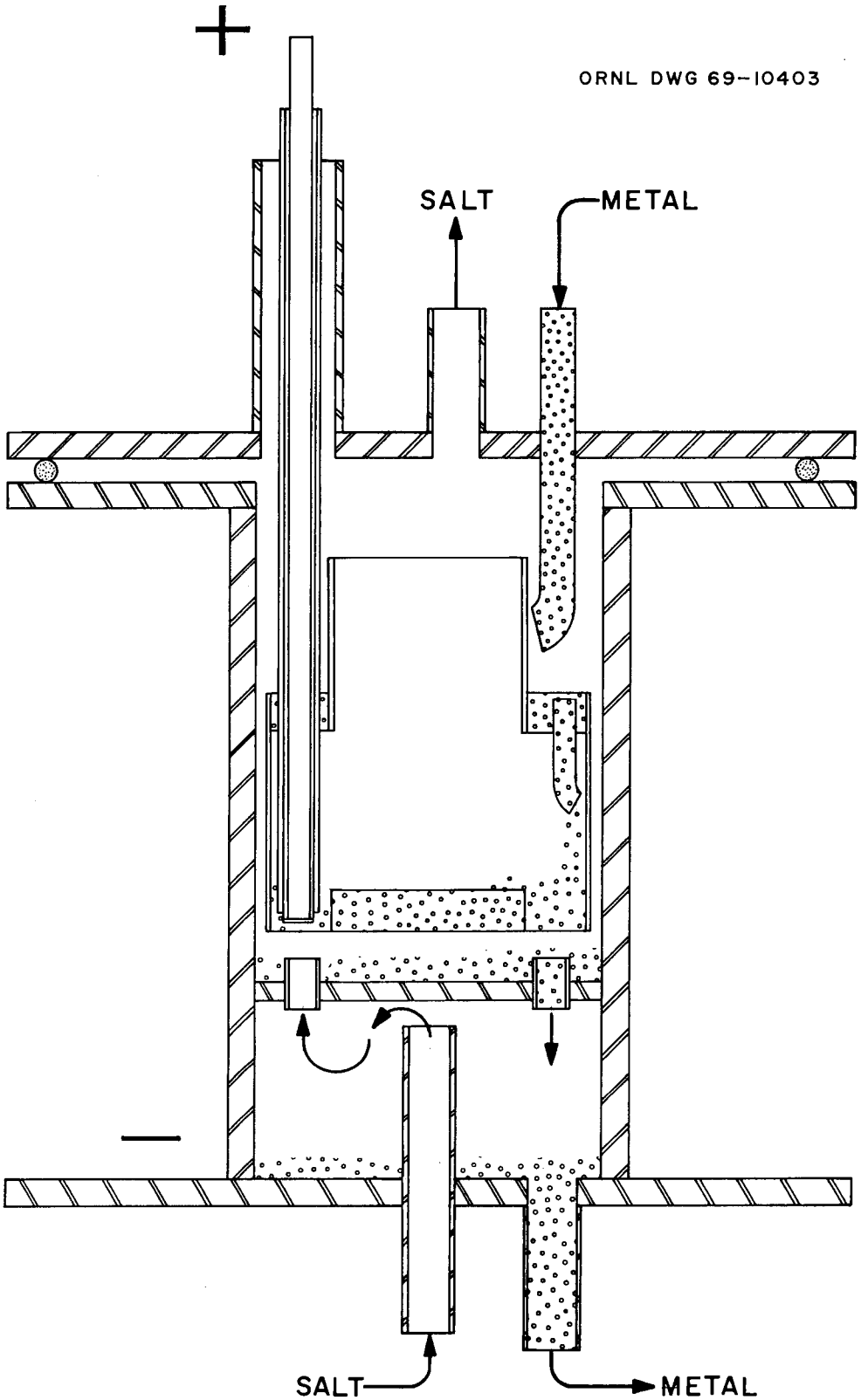

Fig. 3.16. Schematic Diagram of Electrolytic Cell.

sleeve. The rod and the sleeve are sealed at the top with silicone rubber; and the sleeve-and-rod assembly is inserted into a short Teflon sleeve, which is held in place at the top of the 3/4-in. tube by means of a reducing union.

The excess bismuth from the anode flows to the cathode. The reductant-rich effluent from the cathode flows out the bottom of the cell. Salt enters the cell at the bottom, passes through the risers at the cathode and the inner space of the anode and the flow splitter, and leaves the cell at the top.

The cell will be used for the following purposes:

1. To establish the limiting current density by means of current-vs-voltage measurement at several metal and salt flow rates.

2. To find the current efficiency at various current densities, and to determine the salt and metal flow rates by monitoring the flow rates, the current input, and the concentration change in the metal stream.

3. To note the effect on temperature distribution in the cell of heat generation caused by cell resistance. The rate of heat generation caused by the internal resistance is:

$$\frac{W}{v} = I^2\rho,$$

where W/v is the heat generation rate in w/cc, ρ is the resistivity of the salt in ohm-cm, and I is the current density across the electrolyte. The resistivity of the salt under consideration is about 0.5 ohm-cm.[14] At 10 amp/cm^2, the heat generation rate is 50 w/cc.

[14] MSR Program Semiann. Progr. Rept. Aug. 31, 1968, ORNL-4344, p. 163.

Although quartz has been used both as the electrical insulator and as the container for the anode compartment, this material would not be suitable for long-term usage because of the formation of volatile SiF_4.[15,16] It is anticipated that a layer of frozen salt will be used to protect the anodic areas of a cell and to provide electrical insulation. The formation of frozen-salt layers inside a tube has been successfully demonstrated (see Sect. 3.2). The feasibility of forming a salt layer between two flanges (initially spaced with a Teflon O-ring as shown in Fig. 3.17) to electrically insulate the two flanges has also been demonstrated. The flange gap was approximately 1/8 in. when the vessel was assembled. Flinak (liquidus temperature, 454°C) was used as the test salt. During the test, the molten salt was maintained at 1.75 to 2 in. above the gap between the flanges. The salt was maintained at around 500°C for 24 hr; the extent of salt penetration into the gap between the flanges ranged from 0 to 0.75 in. (average 5/16 in.). The salt and the Teflon O-ring were not in direct contact. Electrical resistance was low when the salt was molten, but was very high when the salt was frozen.

Another requirement in the design configuration (Fig. 3.16) is that the flow of bismuth from anode to cathode must be dispersed to ensure that no electrical short circuit occurs between the two electrodes. A preliminary test using mercury and water indicated that dropwise flow could be obtained with mercury flowing at rates up to about 14 cc/min through a section of 2.5-mm-ID, 2-in.-long glass capillary having a 1-cm ID stand tube (arranged as shown in Fig. 3.18). At higher flow rates, an intermittent flow (a period of continuous flow followed by no flow) was observed.

The electromagnetic "pinch effect" has also been considered as a means for producing dropwise flow. An experiment (Fig. 3.19) using a mercury--4 N KBr system will be used to test the concept. The resistivity of the 4 N

---

[15] C. E. Bamberger *et al.*, ORNL-4191 (December 1967), p. 137.

[16] *Reactor Chem. Div. Ann. Progr. Rept. Dec. 31, 1967*, ORNL-4229, p. 60.

ORNL DWG 69-10411

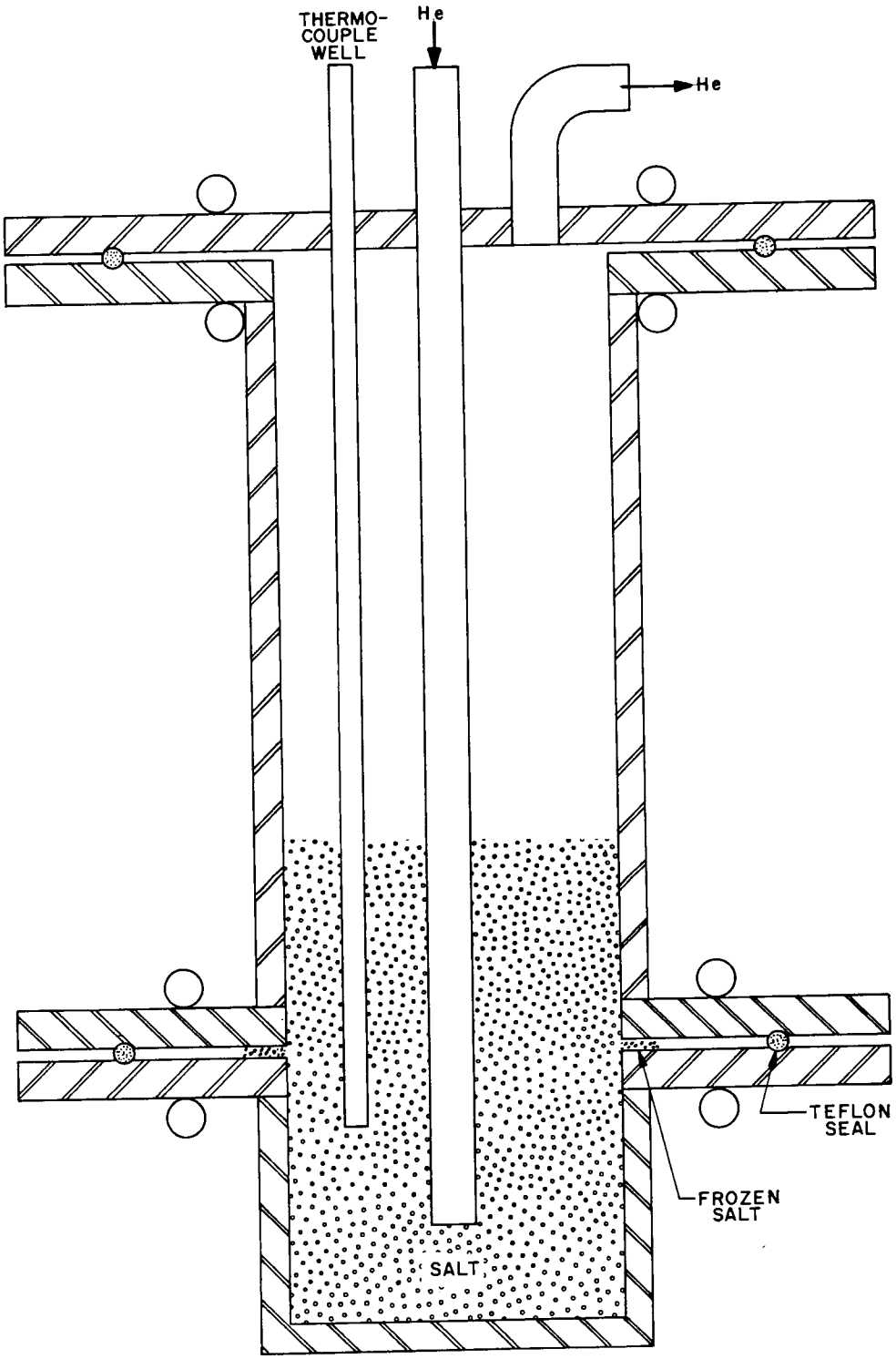

Fig. 3.17. Schematic Diagram of Insulating Flanges.

ORNL DWG 69-10409

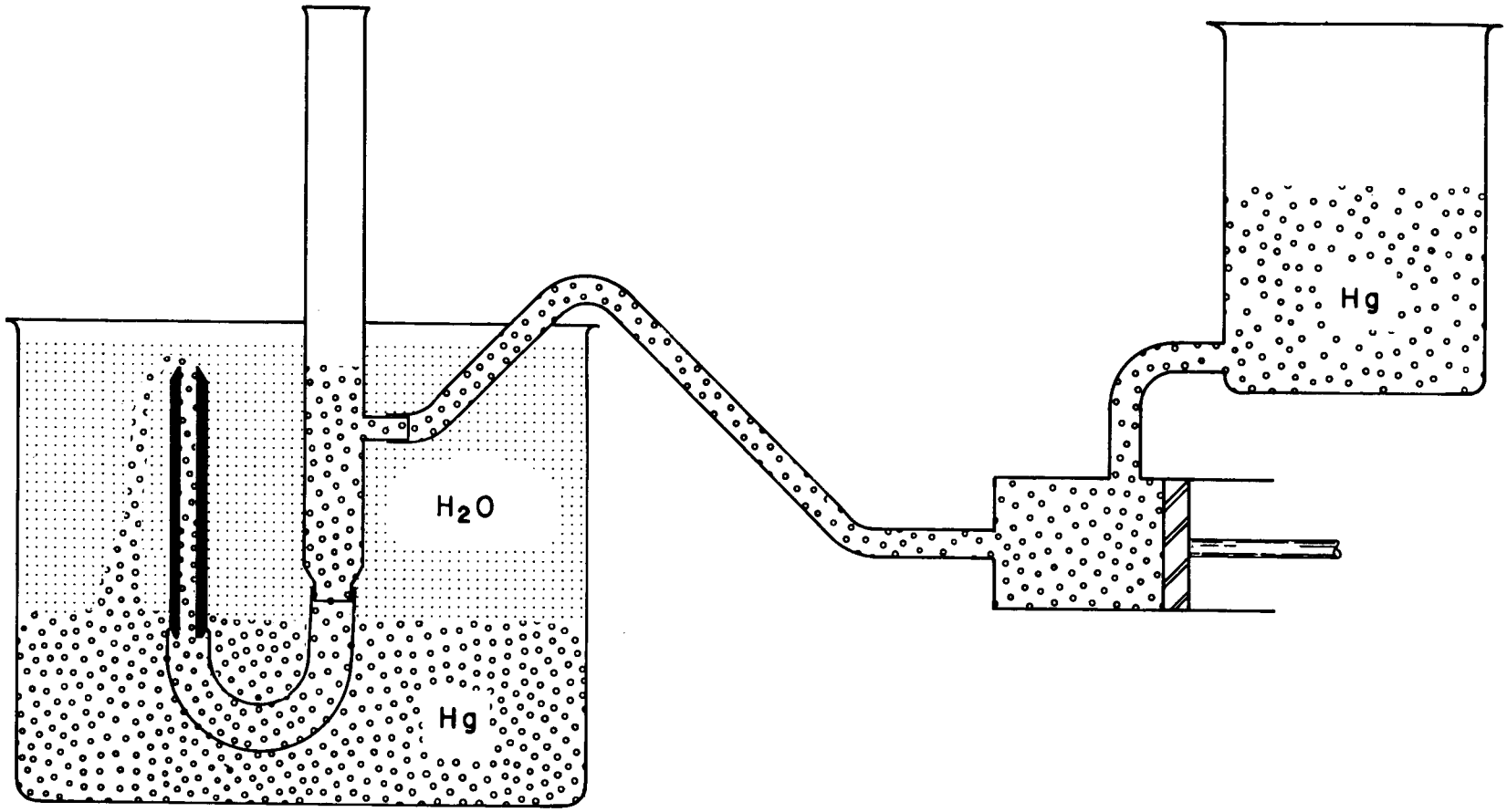

Fig. 3.18. Schematic Diagram of Equipment Used for Study of Prevention of Streaming Flow of a Liquid Metal.

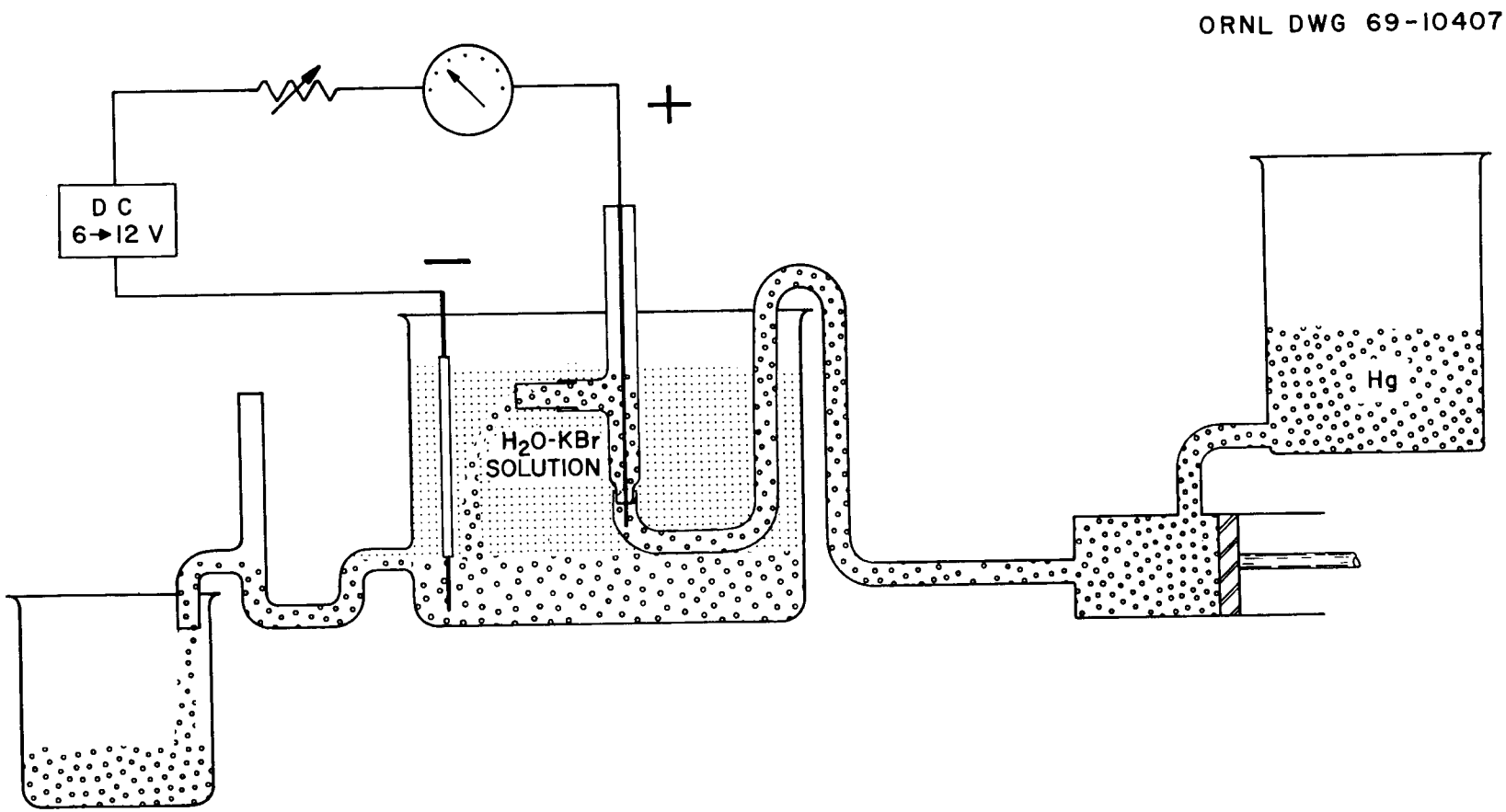

Fig. 3.19. Schematic Diagram of Streaming Flow System Showing Power Supply.

KBr aqueous solution is about 2.9 ohm-cm.[17] A continuous stream of mercury will be maintained through a capillary so that the capillary will be electrically shorted to the mercury pool in the cell. Electric current will then be applied, and the effect of the current upon the mercury flow will be observed. An oscilloscope will be used to observe the wave form of the applied voltage; this will allow us to determine when interruptions occur.

---

[17] J. H. Perry, Chemical Engineer's Handbook, 3d ed., p. 1783, McGraw-Hill, New York, 1949.

ORNL-4365
UC-4 — Chemistry

INTERNAL DISTRIBUTION

1. Biology Library
2-4. Central Research Library
5-6. ORNL — Y-12 Technical Library
Document Reference Section
7-40. Laboratory Records Department
41. Laboratory Records, ORNL R.C.
42. R. E. Blanco
43. J. O. Blomeke
44. R. E. Brooksbank
45. K. B. Brown
46. F. R. Bruce
47. W. D. Burch
48. W. H. Carr
49. G. I. Cathers
50. J. M. Chandler
51. W. E. Clark
52. K. E. Cowser
53. D. J. Crouse
54. F. L. Culler, Jr.
55. W. Davis, Jr.
56. D. E. Ferguson
57. L. M. Ferris
58. J. R. Flanary
59. H. E. Goeller
60. J. M. Googin (Y-12)
61. H. B. Graham
62. A. T. Gresky
63. P. A. Haas
64. F. E. Harrington
65. R. F. Hibbs
66. R. W. Horton
67. G. Jasny (Y-12)
68. H. F. Johnson
69. W. H. Jordan
70. S. H. Jury
71. L. J. King
72. B. B. Klima
73. E. Lamb
74. D. M. Lang
75. R. E. Leuze
76. R. B. Lindauer
77. H. G. MacPherson
78. G. M. Marrow (Y-12)
79. J. L. Matherne
80. J. P. McBride
81. W. T. McDuffee
82. W. H. McVey
83. J. P. Nichols
84. E. L. Nicholson
85. F. L. Parker
86. J. R. Parrott
87. J. H. Pashley (K-25)
88. F. S. Patton, Jr. (Y-12)
89. R. H. Rainey
90. A. D. Ryon
91. W. D. Schaffer, Jr.
92. M. J. Skinner
93. Martha Stewart
94. J. C. Suddath
95. D. A. Sundberg
96. W. E. Unger
97-117. Unit Operations Section
118. C. D. Watson
119. A. M. Weinberg
120. M. E. Whatley
121. R. H. Winget
122. R. G. Wymer
123. E. L. Youngblood
124. P. H. Emmett (consultant)
125. J. J. Katz (consultant)
126. J. L. Margrave (consultant)
127. E. A. Mason (consultant)
128. R. B. Richards (consultant)

EXTERNAL DISTRIBUTION

129. E. L. Anderson, Atomic Energy Commission, Washington
130. A. L. Babb, University of Washington
131. F. P. Baranowski, Atomic Energy Commission, Washington
132. W. G. Belter, Atomic Energy Commission, Washington
133. S. Bernstein, Union Carbide Corporation, Paducah
134. J. M. Berty, Research and Development Department, Union Carbide Corporation, P. O. Box 8361, South Charleston, West Virginia 25314

135. D. E. Bloomfield, Battelle Northwest, Richland, Washington
136. J. A. Buckham, Idaho Chemical Processing Plant
137. J. T. Christy, Richland Operations Office
138. C. R. Cooley, Pacific Northwest, Richland, Washington
139. Kermit Laughon, ORNL, RDT Site Office
140. E. R. Gilliland, Massachusetts Institute of Technology
141. W. W. Grigorieff, Assistant to the Executive Director, Oak Ridge Associated Universities
142. M. J. Harmon, Pacific Northwest, Richland, Washington
143. L. P. Hatch, Brookhaven National Laboratory
144. O. F. Hill, Pacific Northwest, Richland, Washington
145. C. H. Ice, Savannah River Laboratory
146. E. R. Irish, Pacific Northwest, Richland, Washington
147. B. M. Legler, Idaho Chemical Processing Plant
148. J. A. Lieberman, Atomic Energy Commission, Washington
149. B. Manowitz, Brookhaven National Laboratory
150. J. A. McBride, DML, Atomic Energy Commission, Washington
151. J. W. Nehls, Atomic Energy Commission, Oak Ridge
152. C. M. Nicholls, AERE, Harwell, England
153. E. O. Nurmi, Babcock and Wilcox Company
154. H. Pearlman, Atomics International
155. A. M. Platt, Pacific Northwest, Richland, Washington
156. R. A. Proebstle, Knolls Atomic Power Laboratory
157. J. W. Pollock, Idaho Operations Office
158. K. L. Rohde, Idaho Chemical Processing Plant
159. C. A. Rohrmann, Pacific Northwest, Richland, Washington
160. C. M. Slansky, Idaho Chemical Processing Plant
161. M. Smutz, Ames Laboratory, Ames, Iowa
162. C. E. Stevenson, Idaho Division, Argonne National Laboratory, P. O. Box 2528, Idaho Falls, Idaho
163. K. G. Steyer, General Atomic
164. J. A. Swartout, Union Carbide Corporation, New York
165. C. D. Tabor, Goodyear Atomic
166. V. R. Thayer, Du Pont, Wilmington
167. R. C. Vogel, Argonne National Laboratory, 9700 South Cass Ave., Argonne, Illinois
168. G. H. Wagner, General Electric Company, Santa Clara, California
169. D. C. Webster, Associate Director of Chemical Engineering Division, Argonne National Laboratory, 9700 South Cass Ave., Argonne, Illinois
170. Laboratory and University Division, AEC, ORO

171-363. Given distribution as shown in TID-4500 under Chemistry category (25 copies — CFSTI)